NASA TECHNICAL MEMORANDUM 107588

APPLICATION OF FIBER BRIDGING MODELS TO FATIGUE CRACK GROWTH IN UNIDIRECTIONAL TITANIUM MATRIX COMPOSITES

J. G. Bakuckas, Jr. and W. S. Johnson

JULY 1992

National Aeronautics and Space Administration

Langley Research Center
Hampton, Virginia 23665-5225

Abstract

Several fiber bridging models were reviewed and applied in this research to study the matrix fatigue crack growth behavior in center notched $[0]_8$ SCS-6/Ti-15-3 and $[0]_4$ SCS-6/Ti-6Al-4V laminates. Observations revealed that fatigue damage consisted primarily of matrix cracks and fiber-matrix interfacial failure in the $[0]_8$ SCS-6/Ti-15-3 laminates. Fiber-matrix interface failure included fracture of the brittle reaction zone and cracking between the two carbon rich fiber coatings. Intact fibers in the wake of the matrix cracks reduce the stress intensity factor range. Thus, an applied stress intensity factor range ($\Delta K_{app} = \Delta S\sqrt{\pi a}$) is inappropriate to characterize matrix crack growth behavior. Fiber bridging models were used to determine the matrix stress intensity factor range in titanium metal matrix composites. In these models, the fibers in the wake of the crack are idealized as a closure pressure. An unknown constant frictional shear stress is assumed to act along the debond or slip length of the bridging fibers. In this study, the frictional shear stress was used as a curve fitting parameter to available data (crack growth data, crack opening displacement data, and debond length data). Large variations in the frictional shear stress required to fit the experimental data indicate that the fiber bridging models in their present form lack predictive capabilities. However, these models provide an efficient and relatively simple engineering method for conducting parametric studies of the matrix crack growth behavior based on constituent properties.

Nomenclature

a, a_o	Current crack length and unbridged initial crack length, mm
AA'	Superscript referring to crack centerline
A_f, A_m	Cross sectional area of fiber and matrix, m^2
BB'	Superscript referring to end line of slip region
C, n	Paris crack growth coefficient constants, $\sqrt{m}$/MPa*cycle
E_f, E_m	Fiber and matrix modulus, MPa
E_L	Composite longitudinal modulus, MPa
E_T	Composite transverse modulus, MPa
G_{LT}	Composite shear modulus, MPa
ΔK	Mode I stress intensity factor range, MPa$\sqrt{m}$
ΔK_{app}	Applied stress intensity factor range, MPa$\sqrt{m}$
ΔK_m	Discrete stress intensity factor range in matrix, MPa$\sqrt{m}$

ΔK_{tip}	Continuum stress intensity factor range in composite, MPa$\sqrt{m}$
ℓ	Slip length, m
ℓ_R	Slip length of frictional shear stress reversal, m
max	Superscript referring to maximum applied load
min	Superscript referring to minimum applied load
ΔP	Range in closure pressure, MPa
r	Fiber radius, m
R	Stress ratio = S_{min}/S_{max}
ΔS	Applied stress range, MPa
v_f, v_m	Fiber and matrix volume fractions
$\bar{x}$	Integration variable along crack from center, mm
$\Delta\delta_m$	Discrete crack opening displacement range in matrix, μm
$\Delta\delta_{tip}$	Continuum crack opening displacement range in composite, μm
γ_c	Composite fracture surface energy = K_{tip}^2 / E_L, MPa*m
γ_m	Matrix fracture surface energy = K_m^2 / E_m, MPa*m
τ	Interfacial frictional shear stress, MPa
τ_{cg}	Frictional shear stress used to fit the crack growth data, MPa
τ_{cod}	Frictional shear stress used to fit the crack opening displacement data, MPa
τ_{dl}	Frictional shear stress used to fit the debond length data, MPa
ν_{LT}	Composite Poisson's ratio
σ_f, σ_m	Axial stress in fiber and matrix, MPa

Introduction

Fatigue damage progression in advanced titanium matrix composites (TMC) must be properly characterized for these materials to be confidently used in a man-rated aircraft. Numerous investigations have been conducted on the fatigue damage growth behavior in TMC containing stress concentrations (see for example [1-9]). In general, fatigue damage is a complex process which depends on many variables including constituent properties, lay-up, fabrication processes, applied loadings, and specimen geometries. The dominant mechanisms of fatigue damage in TMC are fiber breakage, matrix cracking, and fiber-matrix debonding. Typically, the onset of fiber breakage results in rapid, self-similar damage progression and Mode I, catastrophic fracture [1-3]. Under loading conditions where fibers do not break, damage progression consists primarily of matrix cracking and fiber-matrix debonding [4-9].

Extensive damage with multiple matrix cracks growing parallel to each other has been observed in TMC subjected to maximum loads as low as 17% of the static notched strength [5-8]. Even though the fibers are intact, matrix cracking and fiber-matrix debonding significantly reduced the composite longitudinal stiffness and strength [7,9]. In addition, both composite toughness and environmental protection of the fibers are lost due to matrix cracking. Thus, matrix cracking is of particular concern.

Conventional fracture mechanics characterization of Mode I fatigue crack growth behavior is accomplished through the relation between the crack growth rate and the stress intensity factor range. The most common relation is the power law function proposed by Paris et al. [10]:

$$\frac{da}{dN} = C(\Delta K)^n \tag{1}$$

where C and n are material constants and ΔK is the Mode I stress intensity factor range. To apply Equation (1) to matrix fatigue cracking in TMC requires the appropriate definitions of ΔK, C, and n. Ideally, the values of C and n should be identical to those for the neat matrix material. Typically, ΔK is equal to the applied stress intensity factor range:

$$\Delta K_{app} = \Delta S \sqrt{\pi a} \tag{2}$$

where ΔS is the applied far-field stress range. However, matrix cracking in TMC is unlikely to be governed solely by ΔK_{app}. The stress intensity factor range experienced by the matrix material (ΔK_m) should be a more suitable definition for ΔK.

Expressions for ΔK_m for matrix cracks bridged by intact fibers in an unidirectional composite were derived in several fiber bridging models [11-15]. As illustrated in Figure 1, these models assume that the fiber-matrix interface debonds as matrix cracks progress past the intact fibers. The models also assume that a constant, but unknown, frictional shear stress acts over a slip length in the debond region. The slip length does not necessarily have to be equal to the debond length. An energy balance approach was used by Aveston et al. [11] and Budiansky at al. [12] to derive an expression for K_m in terms of the composite microstructural parameters (constituent moduli, fiber volume fraction, unknown constant

frictional shear stress, etc.) under conditions of steady state cracking during monotonic loading. The steady state stress intensity factor derived in [11,12] is independent of crack length. These two models are referred to as steady state fiber bridging (SSFB) models.

Another class of models, the generalized fiber bridging (GFB) models, combine a continuum fracture mechanics analysis and a micromechanics analysis to derive stress intensity factor solutions for matrix cracks of arbitrary size. In the GFB models, the constraint due to the intact fibers in the wake of the matrix crack is idealized as an unknown closure pressure. The governing equation in terms of the unknown closure pressure is obtained by combining the crack opening displacement solutions from the continuum fracture mechanics analysis and from the micromechanics analysis. The GFB models developed by Marshall et al. [13] and McCartney [14] were formulated for monotonic loading conditions and were modified for fatigue loading conditions by McMeeking and Evans [15]. The GFB models differ from each other in the formulations used to relate the continuum fracture mechanics analysis and the micromechanics analysis. As the crack length increases, K_m asymptotically approaches the steady state value given by the SSFB models.

The objective of this research is to determine the applicability of the GFB models for characterizing matrix fatigue crack growth in center notched $[0]_8$ SCS-6/Ti-15-3 and $[0]_4$ SCS-6/Ti-6Al-4V laminates. The SCS-6/Ti-15-3 laminates were tested as part of the current study and the SCS-6/Ti-6Al-4V laminates were tested by Davidson [16]. Matrix crack initiation and progression were monitored and recorded during fatigue loading. The effect of fiber bridging on the matrix stress intensity factor range, the crack opening displacement, and the debond length were predicted using the GFB models. The unknown frictional shear stress in the GFB models was used as a curve fitting parameter. Calculations of the slip length and the crack opening displacement were compared with those measured in [16]. In addition, calculations of the slip length were compared to debond lengths measured in this study. The Slip lengths in the GFB models were assumed to be equivalent to the debond lengths in this study.

Materials and Test Procedures

Materials and Specimens

The material tested in this study, designated SCS-6/Ti-15-3, is a titanium matrix composite reinforced with continuous silicon-carbide fibers. The composition of the titanium alloy is Ti-15V-3Cr-3Al-3Sn. The composite laminates were fabricated by Textron by hot isostatic pressing (HIPing) Ti-15-3 foils between unidirectional tapes of silicon-carbide (SCS-6) fibers having a diameter of 0.14 mm. The $[0]_8$ laminates had a fiber volume fraction v_f of 0.33 and were in the as-fabricated condition. Table 1 lists the material properties for the SCS-6/Ti-15-3 laminates.

Two SCS-6/Ti-15-3 specimens were cut using a diamond wheel saw into straight-sided coupons with the 0° fibers in the loading direction. Each specimen was 152.4-mm long and 1.8-mm thick. Two notch length-to-width ratios (2a/W) were used, 0.30 and 0.35. The center notches were made using electro-discharge machining (EDM). To make optical observations and replicas, the surface of each specimen was polished to obtain a flat and lustrous finish. Aluminum end tabs were bonded on all specimens to prevent specimen failure in the grips.

Test Procedures

Constant amplitude, tension-tension fatigue tests were conducted under load control with R = 0.1 (S_{min}/S_{max}) at a frequency of 10 Hz using a closed-loop servo-hydraulic test machine equipped with hydraulic grips. Matrix crack initiation and progression were monitored and recorded in real time using a closed-circuit television system (CCTV) having magnification capabilities up to 325X. Testing was periodically interrupted when significant increments in crack extension were observed to take surface replicas and to examine the specimens surface using a scanning electron microscope (SEM) and an optical microscope. In one specimen, the applied stress level was increased after a prescribed number of fatigue cycles while in the second specimen, the applied stress was held constant. The loading history of both specimens is given in Table 2. After fatigue loading, the surface of Specimen 1 was polished to the midplane of the outer ply of fibers. The mechanisms of fiber-matrix interfacial debonding were identified and the debond lengths were measured using the SEM.

Analytical Models

The GFB models [13-15] incorporate the dominant fatigue failure mechanisms typically observed in TMC, namely, matrix cracking and fiber-matrix debonding. Thus, these models appear to be ideally suited to predict the matrix crack growth in TMC. The GFB models combine a continuum fracture mechanics analysis and a micromechanics analysis to obtain expressions for the crack opening displacement and stress intensity factor for matrix cracks bridged by fibers in a unidirectional composite. In the continuum fracture mechanics analysis, crack opening displacement is obtained by modeling the constraint of the bridging fibers as a closure pressure. The crack opening displacement is related to this closure pressure using the micromechanics analysis and discrete-continuum relations. The governing equation reduces to a single nonlinear integral equation in terms of the unknown closure pressure.

In this section, the derivation of the governing equation is described. First, the continuum fracture mechanics and micromechanics analyses are presented. Then, the three discrete-continuum relations, designated MCE, MC and ME formulated by Marshall et al. [13], McCartney [14], and McMeeking and Evans [15], respectively, are reviewed. Finally, these relations are used to combine the continuum fracture mechanics analysis and micromechanics analysis to obtain the governing equation.

Continuum Fracture Mechanics Analysis

The continuum solution is obtained by superimposing the solutions of a crack subjected to a far-field applied stress range, ΔS, and a crack subjected to a change in closure pressure, $\Delta P(x)$, as shown in Figure 1. The origin of the x-y coordinate system is located at the center of the crack. For a composite material, the crack opening displacement is reduced to a single integral equation [17]:

$$\Delta\delta_{tip} = \frac{4\Delta S}{E'}\sqrt{a^2-x^2} + \frac{4}{E'\pi}\int_{a_0}^{a}\Delta P(\tilde{x})\log\left|\frac{\sqrt{a^2-x^2}+\sqrt{a^2-\tilde{x}^2}}{\sqrt{a^2-x^2}-\sqrt{a^2-\tilde{x}^2}}\right| d\tilde{x} \qquad (3)$$

where a_0 is the initial crack length without fiber bridging, a is the final crack length, and E' for an orthotropic material containing a crack normal to the loading direction is [18]:

$$\frac{1}{E'} = \frac{1}{2E_L}\left(\sqrt{2\left\{\sqrt{\frac{E_L}{E_T}} - \nu_{LT}\right\} + \frac{E_L}{G_{LT}}}\right) \tag{4}$$

The terms in this equation are the composite laminate properties as defined in the Nomenclature. For an isotropic material under plane stress conditions, E' is simply equal to the modulus of the material. In several studies [2,4,13,14,19,20], E' in Equation (3) was replaced by the longitudinal modulus of the composite, E_L. However, in this study E' is correctly defined by Equation (4). The composite stress intensity factor range for the problem in Figure 1 is [17]:

$$\Delta K_{tip} = \Delta S\sqrt{\pi a} + 2\sqrt{\frac{a}{\pi}}\int_{a_o}^{a}\frac{\Delta P(x)\,dx}{\sqrt{a^2-x^2}} \tag{5}$$

The quantities $\Delta\delta_{tip}$ and ΔK_{tip} are referred to as the *continuum* crack opening displacement and the *continuum* stress intensity factor range, respectively, for a composite subjected to fatigue loading and can be determined by knowing the closure pressure, $\Delta P(x)$. The quantities $\Delta\delta_{tip}$ and $\Delta P(x)$ are related to each other using the micromechanics analysis and the discrete-continuum relations described in the following sections.

Micromechanics Analysis

The schematic in Figure 2a illustrates the fiber stress along the crack center line, $\Delta\sigma_f^{AA'}$, as a function of the matrix crack opening displacement, $\Delta\delta_m$, during fatigue loading. Three regions are shown: (1) initial loading, O-A; (2) unloading, A-B; and (3) reloading, B-A. Marshall and Oliver [21] derived relations for each of these three regions and made comparisons with results from fiber push-out tests of ceramic matrix composites. McMeeking and Evans [15] used a similar force balance approach to determine the $\Delta\delta_m - \Delta\sigma_f^{AA'}$ relation. The micromechanics analysis provides the vital link between the *discrete* matrix crack opening displacement, $\Delta\delta_m$, and the fiber stress along the matrix crack centerline, $\Delta\sigma_f^{AA'}$, as shown in the Appendix. The unknown closure pressure and the fiber stress along

the matrix crack centerline, $\Delta\sigma_f^{AA'}$, are related through the fiber volume fraction [13-15]:

$$\Delta P = v_f (\Delta\sigma_f^{AA'}) \tag{6}$$

This equation is valid if the fibers are closely spaced relative to the crack length. Using Equation (6), the matrix crack opening displacement is related to the unknown closure pressure:

$$\Delta\delta_m = \lambda \Delta P^2 \tag{7}$$

where:

$$\lambda = \frac{r}{4\tau v_f^2 E_f \eta} \tag{8}$$

and:

$$\eta = \left\{1 + \frac{E_f v_f}{E_m v_m}\right\} \tag{9}$$

Equations (6) and (7) are valid in the wake regions away from the crack-tip; however, the singularity fields in the crack-tip vicinity are not included in the micromechanics analysis. Consequently, Equations (6) and (7) erroneously suggest that the fiber stress vanishes at the crack-tip.

Discrete-Continuum Relations

The continuum fracture mechanics analysis and the micromechanics analysis are combined using the following two discrete-continuum relations: (1) $\Delta\delta_m - \Delta\delta_{tip}$, and; (2) $\Delta K_m - \Delta K_{tip}$. Differences among the GFB models [12-14] arise in defining these two discrete-continuum relations as discussed next.

Crack Opening Displacements

Marshall et al. [13] and McMeeking and Evans [15] assumed that the discrete and the continuum crack opening displacements were equal:

$$\Delta\delta_m = \Delta\delta_{tip} \tag{10}$$

McCartney [14] reported that $\Delta\delta_{tip}$ is actually the change in displacement within the slip region (change in displacement between lines AA' and BB', Figures 2b and 2c) and should be related to $\Delta\delta_m$ as follows:

$$\Delta\delta_m = \Delta\delta_{tip}\eta \tag{11}$$

where η is defined in Equation (9). Both relations are examined in the present study.

Stress Intensity Factor

In order to use a criterion for matrix cracking, a relation between the matrix and continuum stress intensity factors must be established. Marshall et al. [13] related ΔK_m to ΔK_{tip} using the ratio of the matrix modulus to composite modulus:

$$\Delta K_m = \frac{E_m}{E_L}\Delta K_{tip} \tag{12}$$

This equation assumes that the near-tip strains in the composite and in the matrix are compatible. In a different approach, McCartney [14] used an energy balance to relate ΔK_m to ΔK_{tip} by assuming:

$$\gamma_c = v_m\gamma_m \tag{13}$$

where $\gamma_c = K_{tip}^2/E_L$ is the fracture surface energy of the composite and $\gamma_m = K_m^2/E_m$ is the fracture

surface energy of the matrix. Rewriting Equation (13) in terms of stress intensity factor ranges:

$$\Delta K_m = \sqrt{\frac{E_m}{v_m E_L}}\,\Delta K_{tip} \tag{14}$$

Finally, it was suggested by McMeeking and Evans [15]:

$$\Delta K_m = \Delta K_{tip} \tag{15}$$

All three stress intensity factor relations, Equations (12), (14), and (15), are examined in this study.

In the subsequent sections, the discrete-continuum relations derived by Marshall et al. [13] ($\Delta\delta_m = \Delta\delta_{tip}$ and $\Delta K_m = \frac{E_m}{E_L}\Delta K_{tip}$), McCartney [14] ($\Delta\delta_m = \Delta\delta_{tip}\eta$ and $\Delta K_m = \sqrt{\frac{E_m}{v_m E_L}}\,\Delta K_{tip}$) and McMeeking and Evans [15] ($\Delta\delta_m = \Delta\delta_{tip}$ and $\Delta K_m = \Delta K_{tip}$) are referred to as the MCE, MC, and ME relations, respectively.

Governing Equation

The governing crack opening displacement equation is obtained by substituting either Equation (10) or (11) into (3). After normalizing, the governing equation becomes:

$$\underline{P}(u)^2 - \mu\sqrt{1-u^2} = -\frac{\mu}{\pi}\int_c^1 \underline{P}(v)\log\left|\frac{\sqrt{1-u^2}+\sqrt{1-v^2}}{\sqrt{1-u^2}-\sqrt{1-v^2}}\right| dv \tag{16}$$

where:

$\underline{P} = \Delta P/\Delta S$

$u = x/a$

$v = \tilde{x}/a$

$c = a_o/a$

For either the MCE or ME displacement relation (Equation (10)), the term μ is:

$$\mu = \frac{4a}{\lambda E' \Delta S} \tag{17}$$

and for the MC displacement relation (Equation (11)), the term μ is:

$$\mu = \frac{4a}{\lambda E' \Delta S} \eta \tag{18}$$

Equation (16) is a nonlinear integral equation that is solved numerically using an iterative procedure similar to that outlined in [14]. Once the normalized pressure is known, the matrix crack opening displacements are found from either the MCE and ME displacement relations (Equation (10)) or from the MC relation (Equation (11)). Then the matrix stress intensity factor ranges are obtained from the MCE, MC, and ME stress intensity factor relations, Equations (12), (14) and (15), respectively.

Results and Discussions

In this section, the frictional shear stress in the GFB model was used as a curve fitting parameter to matrix crack growth data, debond length data, and crack opening displacement data. The three discrete-continuum relations (i.e. the MCE, MC and ME relations) were used in the analysis. For each TMC system, the experimental results are presented first, followed by the curve fit results using the GFB model. Interpretations of the frictional shear stress term in the GFB model are discussed as well as the differences in the frictional shear stress values used to fit the data. Finally, the limitations and advantages of the GFB model are discussed.

SCS-6/Ti-15-3

Matrix Crack Growth Data

The average cumulative crack extension as a function of the number of cycles is shown in Figure 3 for both SCS-6/Ti-15-3 specimens tested. In Specimen 1 the applied stress level was increased after a

prescribed number of fatigue cycles and in Specimen 2 the applied stress was held constant, as shown in Table 2. In Specimen 1, the crack growth rate increased as the applied stress level increased. For both specimens, the crack growth rate decreased as the crack length increased, as shown in Figure 4.

A typical matrix crack for Specimen 1 subjected to S_{max} = 300 MPa is shown in Figure 5. The crack shown in the first photograph was developed during the previous load history. As shown in this figure, the matrix crack progressed from the notch-tip in a macroscopically self-similar manner. It was assumed that the fibers in the wake of the matrix crack were intact since no jumps in crack opening displacement (COD) were observed and no audible levels of acoustic emission were heard (fiber breakage is associated with sudden increments in COD and high amplitude acoustic emission events [1]). Naik and Johnson [6] also did not observe any fiber breaks in $[0]_8$ SCS-6/Ti-15-3 specimens containing double edge notches subjected to similar loading conditions when the outer layer of matrix material was etched away. The intact fibers in the wake of the matrix crack effectively reduced the crack growth rate as the crack length increased.

The matrix fatigue crack growth behavior in the composite was first characterized using the neat matrix material properties and the applied stress intensity factor range (ΔK_{app}), Equation (2) calculated with standard data reduction procedures (ASTM Standard E647). The crack growth rate (da/dN) as a function of ΔK_{app} for the Ti-15-3 sheet material [22] and the two SCS-6/Ti-15-3 specimens is shown in Figure 6. As shown in this figure, using ΔK_{app} in the composite significantly overestimates the actual stress intensity factor range governing matrix crack growth. In addition, there is a trend towards a negative slope in the da/dN - ΔK_{app} curves for the two composite specimens. For a given ΔK_{app}, the da/dN is reduced by approximately one order of magnitude due mainly to the bridging fibers compared to the neat matrix results.

The GFB models were then used to determine the matrix stress intensity factor range (ΔK_m) in the two specimens tested. Using the unknown frictional shear stress as a curve-fitting parameter, the matrix crack growth data was collapsed onto that of the Ti-15-3 sheet material as shown in Figures 7 through 9. The crack growth data was reduced in Figures 7, 8 and 9 using the MCE, MC and ME relations, respectively. Each figure indicates the discrete-continuum relation used as well as the values of τ_{cg}, the frictional shear stress required to fit the composite crack growth data. As shown in these

figures, the calculated stress intensity factor was reduced when bridging fibers were modeled. In addition, τ_{cg} typically increased as the applied stress increased. There was a wide range in the values of τ_{cg} needed to fit the experimental data, as shown in these figures.

For the specimen subjected to increasing stress levels (Specimen 1), an excellent fit was obtained for each stress level using the value of τ_{cg} shown in Figures 7 through 9. However, for the specimen subjected to a constant applied load (Specimen 2), the fit was not as good for the MC and ME relations, Figures 8 and 9 respectively. In Specimen 1, the crack extensions that occurred during each load level were short compared to that in Specimen 2 (see Table 2). For Specimen 2, a better fit would have been obtained if larger values of τ were used at the higher crack growth rates (corresponding to small crack lengths). This would imply that the frictional shear stress decreases as the crack length increases.

Debond Length Data

In order to study the mechanisms of fiber-matrix debonding, the surface of Specimen 1 near the notch-tip was polished to the midplane of the outer ply and was examined under an SEM. During consolidation, a brittle reaction zone developed between the matrix and the outer of the two carbon rich coatings of the SiC fiber as shown in Figure 10. In the interface of the first intact fiber, the reaction zone near the matrix crack had a rubble-like appearance indicating fracture of the brittle reaction zone. Further away from the matrix crack along the fiber (approximately 0.5 mm away), the reaction zone had a more uniform, intact appearance. However, cracking was now observed between the carbon rich layers. Cracking in the carbon rich layers extended approximately 1.5 mm along the first intact fiber. The transition from fracture of the brittle reaction zone to cracking between the carbon rich coatings occurred approximately 0.42 mm from the crack centerline as shown in Figure 11. In the other bridging fibers, cracking of the carbon rich coating was less prevalent and the debond length was composed mainly of fracture of the brittle reaction zone.

Measurements of the debond length for each fiber in the bridged region are shown for Specimen 1 in Figure 12. The ordinate axis is the distance measured from the first intact fiber. The entire interface damage process zone (failure of reaction zone and cracking in the carbon rich coatings) was assumed to be the debond length. The precise end point of the debond region was difficult to identify; thus, the

results presented in Figure 12 are approximate. As shown in Figure 12, the debond lengths for the fibers in the bridged region decreased as the distance from the first intact fiber increased.

In the GFB models, the slip length is defined as the region over which the frictional shear stress acts. In the present study, the slip length is assumed to be equal to the debond length, and the measured debond lengths are compared to calculated slip lengths. For Specimen 1 the calculated slip lengths are presented in Figures 13 and 14 assuming $\Delta\delta_m = \Delta\delta_{tip}$ (MCE and ME relations) and $\Delta\delta_m = \Delta\delta_{tip}\eta$ (MC relation), respectively. Here, calculations of the slip length are made using several values of frictional shear stress including the values used to fit the crack growth data, τ_{cg}, and the debond length data, τ_{dl}. In Figure 13, the two values of τ_{cg} corresponding to the MCE and ME stress intensity factor relations are labeled. In general, as τ increased, the slip length decreased, where the slip length is proportional to $1/\sqrt{\tau}$. The best agreement between the calculations and experiments was obtained for τ_{dl} = 40 MPa. For all discrete-continuum relations, the debond lengths were overestimated using the corresponding values of τ_{cg} as shown in Figures 13 and 14. The best agreement between τ_{dl} and τ_{cg} was obtained assuming the ME relations [15] (τ_{cg} = 20.43 MPa and τ_{dl} = 40.00 MPa, Figure 13).

As shown in Figures 13 and 14, a better agreement between the measured debond lengths and the calculated slip lengths for the first two fibers in the bridging region would be obtained if smaller values of τ were used. In fact as was shown in Figure 10, the debond length for the first intact fiber consisted mainly of cracking in the carbon rich layers. Although not shown, in the other bridging fibers debonding consisted mainly of fracture of the brittle reaction zone. The crack surfaces in the carbon layers were smoother than the fracture surface in the brittle reaction zone. Hence, in the first intact fiber, it is possible that the overall shear stress acting on the debond surfaces would be lower .

SCS-6/Ti-6Al-4V

Matrix Crack Growth Data

The effects of the frictional shear stress on the matrix crack growth data were determined for the $[0]_4$ SCS-6/Ti-6Al-4V laminate tested in [16]. The reduced matrix crack growth data is shown in Figures 15 , 16, and 17 using the MCE, MC and ME relations, respectively. Here, predictions of the matrix stress intensity factor range are made using several values of frictional shear stress including

values used to fit the crack growth data , τ_{cg}, the debond length data, τ_{dl}, and the crack opening displacement data, τ_{cod}. As shown in these figures, the applied stress intensity factor range overestimates that of the matrix and, therefore, cannot be used to characterize the matrix crack growth behavior. Using the GFB models, the crack growth data for the in situ matrix material and the neat matrix material were forced to coincide by varying τ_{cg}. The best agreements between experiments and predictions were obtained for τ_{cg} = 0.9 MPa, 1.0 MPa, and 4.5 MPa for Figures 15, 16 and 17, respectively. Calculations of the matrix stress intensity factor range was sensitive to the value of τ used. As τ increased, the matrix stress intensity factor decreased, where the matrix stress intensity factor range was proportional to $1/\sqrt{\tau}$. An increase in τ results in an increase in the closure pressure. Consequently, both the crack opening displacement and the stress intensity factor were reduced when τ increased.

Using the MCE and MC relations, the matrix stress intensity factor range was underestimated using τ_{dl} and τ_{cod} as shown in Figures 15 and 16, respectively. The best agreement among the calculations using τ_{dl} , τ_{cod} and τ_{cg} was obtained using the ME relations as shown in Figure 17. In this figure, the experimental values of the crack growth data are bounded by the predictions made using τ_{dl} (lower bound) and τ_{cod} (upper bound). The value of ΔK_m varied approximately ± 3 MPa$\sqrt{m}$ between these bounds.

Debond Length Data

The slip lengths shown in Figures 18 and 19 were calculated assuming $\Delta\delta_m = \Delta\delta_{tip}$ (MCE and ME relations) and $\Delta\delta_m = \Delta\delta_{tip}\eta$ (MC relation), respectively. In these figures, the ordinate axis is the length measured from the first intact fiber. Calculations of the slip length are made using several values of frictional shear stress including τ_{cg}, τ_{dl}, and τ_{cod}. Comparisons are made with the measured debond lengths. In general, the calculated slip length decreased as τ increased, where the calculated slip length was proportional to $1/\sqrt{\tau}$. In Figures 18 and 19, the best fit between the experiments and calculations was obtained for τ_{dl} = 12.5 MPa. In Figure 18, a reasonably good fit was obtained using a single value of the frictional shear stress. However, in Figure 19, a better fit would be obtained if a larger value of τ_{dl} were used for the first two intact fibers in the bridging region. Thus, τ_{dl} is apparently a function of the distance from the first intact fiber for this material as well as the SCS-6/Ti-15-3 tested.

For all discrete-continuum relations, the debond lengths were overestimated using the corresponding values of τ_{cg}, as shown in Figures 18 and 19. In Figure 18, two values of τ_{cg} are labeled corresponding to the MCE and ME stress intensity factor range relations. The best agreement between τ_{dl} and τ_{cg} was found assuming the ME relations (τ_{cg} = 4.5 MPa and τ_{dl} = 12.5 MPa, Figure 18). In this case, the calculated debond lengths using these values of τ_{cg} were approximately twice as large as the experimental measurements, Figure 18. For all three discrete-continuum relations, the debond length was severely overestimated using τ_{cod} as shown in Figures 18 and 19.

Crack Opening Displacement Data

The crack opening displacement shown in Figures 20 and 21 were calculated assuming $\Delta\delta_m = \Delta\delta_{tip}$ (MCE and ME relations) and $\Delta\delta_m = \Delta\delta_{tip}\eta$ (MC relation), respectively. In these figures, the ordinate axis is the length measured from the first intact fiber. Calculations of the crack opening displacement are made using several values of frictional shear stress including τ_{cg}, τ_{dl}, and τ_{cod}. In Figure 20, two values of τ_{cg} are labeled corresponding to the MCE and ME stress intensity factor relations. In general, the calculated crack opening displacements decreased as τ increased. The calculated crack opening displacement was proportional to $1/\tau$. The best fit between experiments and calculations was found for τ_{cod} = 1.5 MPa and τ_{cod} = 3.0 MPa, as shown in Figure 20 and 21, respectively. In both figures, a better fit would have been obtained if larger values of τ_{cod} were used for the first four intact fibers in the bridging region. For all discrete-continuum relations, the crack opening displacement data was underestimated using τ_{dl}. For the MCE and MC relations, the crack opening displacement data was bounded by the calculations made using τ_{dl} and τ_{cg}, Figures 20 and 21, respectively.

Interpretation of Frictional Shear Stress

The unknown constant frictional shear stress used in the fiber bridging models is a critical parameter. As shown previously in Figure 10, cracking of the reaction zone occurs near the matrix crack, but further along the fiber-matrix interface, a transition in the debonding mechanism was observed and cracking between the carbon layers was found. The value of τ should be considerably different in

these two debonded regions. The value of τ used in the GFB models can only represent an average of the actual shear stress distribution acting on the debonded surfaces.

The actual frictional shear stress is a difficult quantity to measure and, thus, it has been frequently used as a curve fitting parameter. However, τ is related to both the debond length and the crack opening displacements, which can be directly measured. The interfacial frictional shear stress can only have some physical significance if the same value of τ can be used to accurately predict the matrix crack driving force, the debond length, and the crack opening displacement. The values of τ used to fit the crack growth data (τ_{cg}), the debond length data (τ_{dl}), and the crack opening displacement data (τ_{cod}) are listed in Table 3 according to the discrete-continuum relation used in the calculation. No crack opening displacement data was measured for the SCS-6/Ti-15-3 laminates tested here. As indicated in this table, there is a large difference in the values of τ_{cg}, τ_{cod} and τ_{dl} even within a specific discrete-continuum relation. Thus, quantifying the frictional shear stress using the GFB models does not appear to be a valid approach.

The ME relations, $\Delta\delta_m = \Delta\delta_{tip}$ and $\Delta K_m = \Delta K_{tip}$, produced the best fit for the data sets in this study and in [16] with the least variation in the frictional shear stress. Using the ME relations, all values of τ were between 4 and 360 MPa, the range of τ reported in [2,15,20,23,24,25,26] for both SCS-6/Ti-15-3 and SCS-6/Ti-6Al-4V, except for the value of τ_{cod} (1.5 MPa) for the SCS-6/Ti-6Al-4V specimen. From fiber push-out tests, the reported range of values of τ was from 30 to 360 MPa [20,25,26] which is an upper limit to the values calculated in this study. The large variation among the reported values of frictional shear stress measured from fiber push-out tests is probably due to differences in test methodologies, composite fabrication procedures, etc. In addition, the measured frictional shear stress values from the fiber push-out tests may not accurately represent the actual shear stress acting along the debond region in a bridging fiber. Thus, comparisons with values of τ calculated in this study may not be appropriate.

Advantages and Limitations of Fiber Bridging Models

The evaluated fiber bridging models do capture the most essential features of the fatigue damage progression in the materials studied, i.e., both matrix cracking and fiber-matrix debonding are modeled.

Thus, an expression for the stress intensity factor range driving the observed matrix cracks was obtained. In addition, these models are relatively simple to program and can be used to determine the severity of damage based on the fiber stress or the matrix stress intensity factor. The matrix fatigue cracking can be effectively characterized without using complicated numerical methods, such as finite element analyses, which can be quite cumbersome.

The GFB models were useful for the parametric studies conducted here and for interpreting experimental results. In another useful application, the effects of fiber-matrix interface strength on the fatigue behavior can be studied by varying τ. The effect of the frictional shear stresses on the stress intensity factor range and the stress in the first intact fiber is shown in Figure 22. As τ increases (increasing fiber-matrix bond strength) the fiber stress increases while ΔK_m decreases. Thus, the fibers would tend to fracture in a composite with a strong fiber-matrix interface, whereas, matrix cracks would more likely propagate in a composite with a weak fiber-matrix interface. This trend agrees with observations made by Naik et al. [28] on the effects of the fiber-matrix interface strength on the fracture and fatigue properties of [0/90/0] SCS-6/Ti-15-3 laminates.

There are several limitations to the fiber bridging models worth noting. The fibers bridging the matrix cracks are idealized as a continuous closure pressure. The micromechanical analysis relating the closure pressure to crack opening displacement is based on a simplified one-dimensional analysis of a fiber in the wake of the matrix crack and does not consider the crack-tip mechanics. The complex micromechanical details at the crack tip are not modeled. Consequently, the fiber stresses calculated using the fiber bridging models vanish at the crack-tip, which is unrealistic. In addition, the fiber bridging models cannot take into account the three dimensional effect of the crack front bowing around the fibers as discussed and modeled by Bower and Ortiz [27]. This toughening mechanism, termed "crack trapping", can considerably reduce the crack driving force. It was shown in [27] that crack trapping can double the toughness of a brittle matrix composite without fiber bridging. Finally, modeling the frictional shear stress as a constant is approximate at best. As discussed earlier, the variation in debonding mechanisms along the interface would certainly yield differences in τ. In addition, the large variation in the values of τ used in fitting the various data sets is quit disturbing. The frictional shear stress is apparently a function of crack length, applied stress, distance from the first intact

fiber, and distance along the debond length, and, thus, is not a material constant.

The predictive capabilities of the GFB models are very suspect due to the dependency of τ on so many factors. However, the GFB models may provide a frame work for a crack growth prediction methodology. This may be accomplished by incorporating the crack-tip singularity fields in the micromechanics analysis and reevaluating the discrete-continuum relations which appear to be over-simplified. In addition, a value of the frictional shear stress should be established through experiments and used in the analysis since it resembles a material parameter. A new fitting parameter can then be introduced in the model to include mechanisms not currently being considered such as crack trapping.

Concluding Remarks

In this study, the application of the generalized fiber bridging (GFB) models to analyze matrix crack growth in $[0]_8$ SCS-6/Ti-15-3 and $[0]_4$ SCS-6/Ti-6Al-4V laminates was investigated. Experimental observations revealed that the fatigue damage in $[0]_8$ SCS-6/Ti-15-3 laminates consisted primarily of Mode I matrix cracks that initiated and grew from notch-tips. Fibers were intact in the wake of the matrix cracks. In addition, fiber-matrix debonding in the form of fracture of the brittle reaction zone and cracking between the two carbon rich fiber coatings was found. Under a constant applied stress range, crack growth rate decreased as the matrix crack length increased. The fibers in the wake of the matrix cracks effectively reduced the stress intensity factor. The applied stress intensity factor range did not characterize the fatigue crack growth of matrix cracks which were bridged by fibers.

The effect of the fibers bridging the matrix crack was studied using the GFB models. In these models, fiber-matrix debonding is modeled as the matrix crack progresses past the fibers. An unknown constant frictional shear stress acts over the debond or slip length. These models derive the matrix stress intensity factor by combining a continuum fracture mechanics analysis and a micromechanics analysis using discrete-continuum relations. In the continuum fracture mechanics analysis, expressions for the composite stress intensity factor range (ΔK_{tip}) and the composite crack opening displacement ($\Delta\delta_{tip}$) are derived. The micromechanics analysis provides the solution to the matrix crack opening displacement ($\Delta\delta_m$) in terms of the unknown closure pressure and the composite micromechanical parameters. Discrete-continuum relations are used to relate ΔK_m to ΔK_{tip} and $\Delta\delta_m$ to $\Delta\delta_{tip}$.

The effect of fiber bridging on the matrix stress intensity factor range, the crack opening displacement, and the debond length were studied using the GFB models. The GFB models were exercised using the unknown constant frictional shear stress, τ, as a curve fitting parameter to available data. In general, as τ increased, the calculated matrix stress intensity factor, crack opening displacement, and slip length all decreased. By assuming $\Delta K_m = \Delta K_{tip}$ and $\Delta \delta_m = \Delta \delta_{tip}$, the GFB models yielded the most accurate correlations based on the smallest scatter in frictional shear stress. However, there was a large difference in the values of τ used to correlate the data even within a specified discrete-continuum relation. The value of τ depended on the crack length, applied stress level, and distance from the first intact fiber and is not a material property.

There are several shortcomings of the GFB models. The fiber bridging models cannot account for the three-dimensional effects such as crack front bowing, which can considerably reduce the matrix stress intensity factor. The GFB models assume the frictional shear stress acting along the debonded fiber-matrix interface is a constant. The different debonding mechanisms observed along the interface should, however, result in a variation in the frictional shear stress. Finally, the predictive capabilities of the GFB models are questionable due to the dependency of τ on many factors.

In spite these limitations, the GFB models do incorporate the major modes of fatigue damage (matrix cracking and fiber-matrix debonding) and yield expressions for the stress intensity factors that characterize the matrix crack driving force. The GFB models provide an efficient and relatively simple engineering approximation to conduct parametric analysis using the composite micromechanical variables.

Acknowledgements

The first author gratefully acknowledges the support extended by the National Research Council, Washington, D.C., through their Associateship Program. Thanks are also due Mr. Scott Willard, Research Engineer, Lockheed Engineering and Sciences Company, Hampton, VA, for his efforts in taking the micrographs using the scanning electron microscope.

References

[1] Bakuckas, J. G. Jr., and Awerbuch, J., "Crack-Tip Damage Progression and Acoustic Emission in Unidirectional Silicon-Carbide/Titanium 6Al-4V Composite," *Proceedings of the Thirteenth International Symposium for Testing and Failure Analysis,* ISTFA/87, Los Angeles, CA, November 9-13, 1987, pp. 33-42.

[2] Walls, D., Bao, G., and Zok, F., "Fatigue Crack Growth in a Ti/SiC Composite," *Mechanical Fatigue of Advanced Materials,* Ritchie, Cox and Dauskardt, Eds., MCEP Publishers, 1991, pp. 343-356.

[3] Bowen, P., Ibbotson, A. R., and Beevers, C. J., "Characterization of Crack Growth in Continuous Fibre Reinforced Titanium Based Composites Under Cyclic Loading," *Mechanical Fatigue of Advanced Materials,* Ritchie, Cox and Dauskardt, Eds., MCEP Publishers, 1991, pp. 379-393.

[4] Kantzos, P. and Telesman, J., "Fatigue Crack Growth Study of SCS6/Ti-15-3 Composite," *Int. J. Fatigue,* Vol 12, No. 5, September 1990, pp. 409-415.

[5] Hillberry, B. M. and Johnson, W. S., "Matrix Fatigue Crack Development in a Notched Continuous Fiber SCS-6/Ti-15-3 Composite," *Symposium on Microcracking Induced Damage in Composites,* ASME Winter Annual Meeting, Dallas, Texas, November 26-28, 1990, pp. 121-127.

[6] Naik, R. A., and Johnson, W. S., "Observations of Fatigue Crack Initiation and Damage Growth in Notched Titanium Matrix Composites," *Third Symposium on Composite Materials: Fatigue and Fracture, ASTM STP 1110,* T. K. O'Brien, Ed., American Society for Testing and Materials, 1991, pp. 753-771.

[7] Bakuckas, J. G. Jr., Johnson, W. S., and Bigelow, C. A.,"Fatigue Damage in Cross-Ply Titanium Metal Matrix Composites Containing Center Holes," *NASA TM 104197,* February 1992.

[8] Harmon, D. M., and Saff, C. R.,"Damage Initiation and Growth in Fiber Reinforced Metal Matrix Composites," *Metal Matrix Composites: Testing, Analysis and Failure, ASTM STP 1032,* W, S. Johnson, Ed., American Society for Testing and Materials, 1989, pp. 237-250.

[9] Johnson, W. S., "Fatigue of Continuous Fiber Reinforced Titanium Metal Matrix Composites," *Mechanical Fatigue of Advanced Materials,* Ritchie, Cox and Dauskardt, Eds., MCEP Publishers, 1991, pp.357-378.

[10] Paris, P. C., Gomez M. P., and Anderson, W. E., "A Rational Analytic Theory of Fatigue," *The Trend in Engineering,* Vol. 13, pp. 9-14, 1961.

[11] Aveston, J., Cooper, G. A., and Kelly, A., "Single and Multiple Fracture," *Conference on the Properties of Fibre Composite, National Physical Laboratory.,* IPC Science and Technology Press, 1971, pp. 15-26.

[12] Budiansky, B., Hutchinson, J. W., and Evans, A. G., "Matrix Fracture in Fiber-Reinforced Ceramics," *J. Mech. Phys. Solids,* Vol. 34, No. 2, 1986, pp. 167-189.

[13] Marshall, D. B., Cox, B. N., and Evans, A. G., "The Mechanics of Matrix Cracking in Brittle-Matrix Fiber Composites," *Acta Metall.,* Vol. 33, No. 11, 1985, pp. 2013-2021.

[14] McCartney, L. N., "Mechanics of Matrix Cracking in Brittle-Matrix Fibre-Reinforced Composites," *Proc. R. Soc. Lond.,* A 409, pp. 329-350, 1987.

[15] McMeeking, R. M., and Evans, A. G., "Matrix Fatigue Cracking in Fiber Composites," *Mechanics of Materials,* Vol. 9, 1990, pp. 217-227.

[16] Davidson, D. L., "Fracture Micromechanics of Intermetallic and Ceramic Matrix Continuous Fiber Composites," *Interim Technical Report 06-8602/6,* Southwest Research Institute, San Antonio, TX 78284, May 1991.

[17] Tada, H., Paris, P. C., and Irwin, G. R., *The Stress Analysis of Cracks Handbook,* Del Research Corporation, St. Louis, MO, 63105, 1985.

[18] Lekhnitskii, S. G., *Theory of Elasticity of an Anisotropic Body,* Holden-Day, San Francisco, 1963.

[19] Marshall, D. B., and Cox, B. N., "Tensile Fracture of Brittle Matrix Composites: Influence of Fiber Strength," *Acta Metall,* Vol. 35, No. 11, 1987, pp. 2607-2619.

[20] Sensmeir, M. D., and Wright, P. K., "The Effect of Fiber Bridging on Fatigue Crack Growth in Titanium Matrix Composites ," *Fundamental Relations Between Microstructure and Mechanical Properties of Metal - Matrix Composites,* P. K. Liaw, and M. N. Gungor, Eds., The Minerals, Metals and Materials Society, 1990, pp. 441 - 457.

[21] Marshall, D. B., and Oliver, W. C., "Measurement of Interfacial Mechanical Properties in Fiber-Reinforced Ceramic Composites," *J. Am. Ceram. Soc.,* Vol. 70, 1987, pp. 542-548.

[22] Lenning, G. A, Hall, J. A., Rosenblum, M. E., and Trepel, W. B., "Cold Formable Titanium Sheet," *AFWAL-TR-82-4174,* December 1982.

[23] Ghosn, L. J., Kantzos, P., and Telesman, J.,"Modeling of Crack Bridging in a Unidirectional Metal Matrix Composite," *NASA TM 104355,* May 1991.

[24] Walls, D., Bao, G., and Zok, F.,"Effects of Fiber Failure on Fatigue Cracking in a Ti/SiC Composite," *Scripta Met.*, Vol 25, 1991, pp. 911-916.

[25] Warren, P., Mackin, T., and Evans, A. G., "Design, Analysis and Application of an Improved Push-Through Test for the Measurement of Interface Properties in Composites," *Acta. Met.*, Vol. 40, No. 6, 1992. pp. 1243-1249.

[26] Yang, C. J., Jeng, S. M., and Yang, J. M., "Interfacial Properties Measurements for SiC Fiber-Reinforced Titanium Alloy Composites," *Scripta Met.*, Vol 24, 1990, pp. 469-474.

[27] Bower, A. F., and Ortiz, M., "A Three-Dimensional Analysis of Cracks Trapping and Bridging By Tough Particles," *J. Mech. Phys. Solids.,* Vol. 39, No. 6, 1991, pp. 815-858.

[28] Naik, R. A., Pollock, W. D., and Johnson, W. S., "Effect of a High-Temperature Cycle on the Mechanical Properties of Silicon Carbide/Titanium Metal Matrix Composites," *J. of Materials Science.,* Vol. 26, 1991, pp. 2913-2920.

[29] Bahei-El-Din, Y. A., and Dvorak, G. J., "Plasticity Analysis of Laminated Composite Plates," *J. Appl. Mech.*, Vol. 49, No. 4, December 1982, pp. 740-746.

Appendix: Micromechanics of Fiber Bridging

The relation between the *discrete* crack opening displacement and the fiber stress along the crack centerline is derived in detail for each region of fatigue loading shown in Figure 2a. A free body diagram of a fiber in the wake of the matrix crack for each loading phase is shown in Figures 2b and 2c.

Loading: O-A

During the initial loading along O-A (Figure 2a), the frictional shear stress (τ) is constant in the slip region (ℓ) and opposes the fiber stress, Figure 2b. This free body diagram is constructed assuming the maximum load is just reached (Point A in Figure 2a). Along line BB' (end of slip region), the strains in the fiber and the matrix are equal:

$$\frac{(\sigma_f^{BB'})^{max}}{E_f} = \frac{(\sigma_m^{BB'})^{max}}{E_m} \tag{A1}$$

where $(\sigma_f^{BB'})^{max}$ and $(\sigma_m^{BB'})^{max}$ are the fiber and matrix stresses along line BB' at the maximum applied load (Point A in Figure 2a). Overall equilibrium in the matrix in the slip region requires:

$$(\sigma_m^{BB'})^{max} A_m - 2\pi\tau r\ell = 0 \tag{A2}$$

where A_m is the cross-sectional area of the matrix. Equilibrium in the fiber in the slip region requires:

$$(\sigma_f^{BB'})^{max} A_f + 2\pi\tau r\ell = (\sigma_f^{AA'})^{max} A_f \tag{A3}$$

where $(\sigma_f^{AA'})^{max}$ is the fiber stress along the matrix crack centerline AA' and A_m is the cross-sectional area of the fiber. Combining Equations (A1), (A2), and (A3), the fiber stress along the crack centerline AA' at the maximum load is:

$$(\sigma_f^{AA'})^{max} = \frac{2\tau\ell}{r}\eta \qquad \text{(A4)}$$

where:

$$\eta = \left\{1 + \frac{E_f v_f}{E_m v_m}\right\} \qquad \text{(A5)}$$

The total extension of the matrix in the slip region is:

$$u^{max} = \int_0^{\ell} \left(\frac{(\sigma_m^{BB'})^{max}}{E_m} - \frac{2\pi\tau r y}{E_m A_m}\right) dy = \frac{\pi\tau r \ell^2}{E_m A_m} \qquad \text{(A6)}$$

and of the fiber:

$$\frac{\delta_m^{max}}{2} + u^{max} = \int_0^{\ell} \left(\frac{(\sigma_f^{BB'})^{max}}{E_f} + \frac{2\pi\tau r y}{E_f A_f}\right) dy = \frac{(\sigma_f^{BB'})^{max}\,\ell}{E_f} + \frac{\pi\tau r \ell^2}{E_f A_f} \qquad \text{(A7)}$$

Combining Equations (A1), (A2), (A6), and (A7), an expression for the slip length, ℓ, is obtained in terms of the crack opening displacement at the maximum load, δ^{max}:

$$\ell = \sqrt{\frac{\delta_m^{max} r E_f}{2\tau\eta}} \qquad \text{(A8)}$$

Substituting Equation (A8) into (A4) yields the relation between the fiber stress along the crack centerline and the discrete crack opening displacement at the maximum applied load:

$$\delta_m^{max} = \frac{r}{2\tau E_f \eta}\left\{(\sigma_f^{AA'})^{max}\right\}^2 \qquad (A9)$$

Unloading: A-B

Upon unloading, the frictional shear stress reverses direction within a length, ℓ_R, in the slip region. The free body diagram, Figure 2c, is constructed assuming the minimum load is just reached (Point B in Figure 2a). The procedure to determine the relation between the fiber stress and discrete crack opening displacement is similar to that at maximum load. Along line BB' (end of slip region), the strains in the fiber and the matrix are equal:

$$\frac{(\sigma_f^{BB'})^{min}}{E_f} = \frac{(\sigma_m^{BB'})^{min}}{E_m} \qquad (A10)$$

Overall equilibrium in the matrix in the slip region requires:

$$(\sigma_m^{BB'})^{min} A_m - 2\pi\tau r(\ell - \ell_R) + 2\pi\tau r\ell_R = 0 \qquad (A11)$$

and in the fiber:

$$(\sigma_f^{BB'})^{min} A_f + 2\pi\tau r(\ell - \ell_R) - 2\pi\tau r\ell_R = (\sigma_f^{AA'})^{min} A_f \qquad (A12)$$

Combining Equations (A10), (A11), and (A12), the fiber stress along the crack centerline at the minimum load is:

$$(\sigma_f^{AA'})^{min} = \frac{2\pi\tau}{R}\eta\,(\ell - 2\ell_R) \qquad (A13)$$

Substituting Equation (A4) into (A13):

$$\Delta\sigma_f^{AA'} = \frac{4\pi\tau}{r}\eta\,\ell_R \tag{A14}$$

where $\Delta\sigma_f^{AA'} = (\sigma_f^{AA'})^{max} - (\sigma_f^{AA'})^{min}$. The total extension of the matrix in the slip region at the minimum load is:

$$u^{min} = \int_0^{\ell-\ell_R} \left(\frac{(\sigma_m^{BB'})^{min}}{E_m} - \frac{2\pi\tau r y}{E_m A_m}\right) dy + \int_{\ell-\ell_R}^{\ell} \left(\frac{(\sigma_m^{BB'})^{min}}{E_m} - \frac{4\pi\tau r(\ell-\ell_R)}{E_m A_m} + \frac{2\pi\tau R\, y}{E_m A_m}\right) dy \tag{A15}$$

which reduces to:

$$u^{min} = \frac{(\sigma_m^{BB'})^{min}\,\ell}{E_m} + \frac{\pi\tau r}{E_m A_m}(-\ell^2 + 2\ell_R{}^2) \tag{A16}$$

The extension of the fiber at the minimum load is:

$$\frac{\delta_m^{min}}{2} + u^{min} = \int_0^{\ell-\ell_R} \left(\frac{(\sigma_f^{BB'})^{min}}{E_f} + \frac{2\pi\tau r\, y}{E_f A_f}\right) dy + \int_{\ell-\ell_R}^{\ell} \left(\frac{(\sigma_f^{BB'})^{min}}{E_f} + \frac{4\pi\tau r(\ell-\ell_R)}{E_f A_f} - \frac{2\pi\tau r\, y}{E_f A_f}\right) dy \tag{A17}$$

which reduces to:

$$\frac{\delta_m^{min}}{2} + u^{min} = \frac{(\sigma_f^{BB'})^{min}}{E_f} + \frac{\pi\tau r}{E_f A_f}(\ell^2 - 2\ell_R^2) \qquad \text{(A18)}$$

Combining Equations (A10), (A11), (A16), and (A18):

$$\delta_m^{min} = \frac{2\tau\eta}{RE_f}(\ell^2 - 2\ell_R^2) \qquad \text{(A19)}$$

By substituting Equation (A8) into (A19), the length of the shear stress reversal at the minimum load is:

$$\ell_R = \sqrt{\frac{rE_f}{4\tau\eta}\Delta\delta_m} \qquad \text{(A20)}$$

where $\Delta\delta_m = \delta_m^{max} - \delta_m^{min}$. Combining Equations (A14) and (A20) yields the relation between the change in fiber stress along the crack centerline and the change in discrete crack opening displacement from points A to B in Figure 2a:

$$\Delta\delta_m = \frac{r}{4\tau E_f \eta}\left\{\Delta\sigma_f^{AA'}\right\}^2 \qquad \text{(A21)}$$

Reloading: B-A

When reloading back to A, the constant frictional shear stress in ℓ_R reverses direction. Upon reaching A, the shear stress within the entire slip length, ℓ, is in the same direction. The free body diagram in this case is the same as that shown for the original loading case, Figure 2b. Consequently, the discrete crack opening displacement when reloaded to Point A is identical to Equation (A9). Moreover, the change in displacement from Point B to A in Figure 2a is the same as that from Point A to B (Equation (A21)).

Table 1. Material Properties:

	Property	SCS-6/Ti-15-3	SCS-6/Ti-6Al-4V [16]
Matrix:	E_m (GPa)	92.4	110.0
	ν_m	0.34	0.34
	C ($\sqrt{m}$/MPa*cycle)	6.49E-11	4.00E-11
	n	2.72	3.00
Fiber:	E_f (GPa)	400.0	400.0
	ν_f	0.25	0.25
Composite:	Laminate	$[0]_8$	$[0]_4$
	v_f	0.33	0.42
	E_L (GPa) [a]	192.2	231.8
	E_T (GPa) [a]	130.1	165.5
	G_{LT} (GPa) [a]	45.9	59.6
	ν_{LT} [a]	0.32	0.30

[a] Predicted based on constituent properties [29]

Table 2. Specimen Loading History:

Specimen Number	a_0 (Initial) (mm)	a_f (Final) (mm)	Applied Stress S_{max} (MPa)	Number of Cycles	
1	3.048	3.254	65	250,000	(precracking)
1	3.254	3.572	120	150,00	
1	3.572	3.745	200	40,000	
1	3.745	4.281	300	50,000	
2	3.316	3.375	65	250,000	(precracking)
2	3.375	5.081	325	250,000	

Table 3. Values of constant frictional shear stress used to fit experimental data

Material and Test Conditions	Data Type	Discrete-Continuum Relations		
		MCE [13]	MC [14]	ME [15]
		$\Delta K_m = \frac{E_m}{E_L}\Delta K_{tip}$ $\Delta\delta_m = \Delta\delta_{tip}$	$\Delta K_m = \sqrt{\frac{E_m}{\nu_m E_L}}\Delta K_{tip}$ $\Delta\delta_m = \Delta\delta_{tip}\eta$	$\Delta K_m = \Delta K_{tip}$ $\Delta\delta_m = \Delta\delta_{tip}$
SCS-6/Ti-15-3 Lay - Up : $[0]_8$ V_f = 0.33 S_{max} = 300 MPa a = 4.28 mm	$\frac{da}{dN} - \Delta K_m$	τ_{cg} = 3.83 MPa	τ_{cg} = 4.90 MPa	τ_{cg} = 20.43 MPa
	$\ell - a$	τ_{dl} = 40.00 MPa	τ_{dl} = 40.00 MPa	τ_{dl} = 40.00 MPa
SCS-6/Ti-6-4 Lay - Up : $[0]_4$ V_f = 0.42 S_{max} = 194 MPa a = 5.97 mm	$\frac{da}{dN} - \Delta K_m$	τ_{cg} = 0.90 MPa	τ_{cg} = 1.00 MPa	τ_{cg} = 4.5 MPa
	$\ell - a$	τ_{dl} = 12.50 MPa	τ_{dl} = 12.50 MPa	τ_{dl} = 12.50 MPa
	$\Delta\delta_m - a$	τ_{cod} = 1.50 MPa	τ_{cod} = 3.00 MPa	τ_{cod} = 1.50 MPa

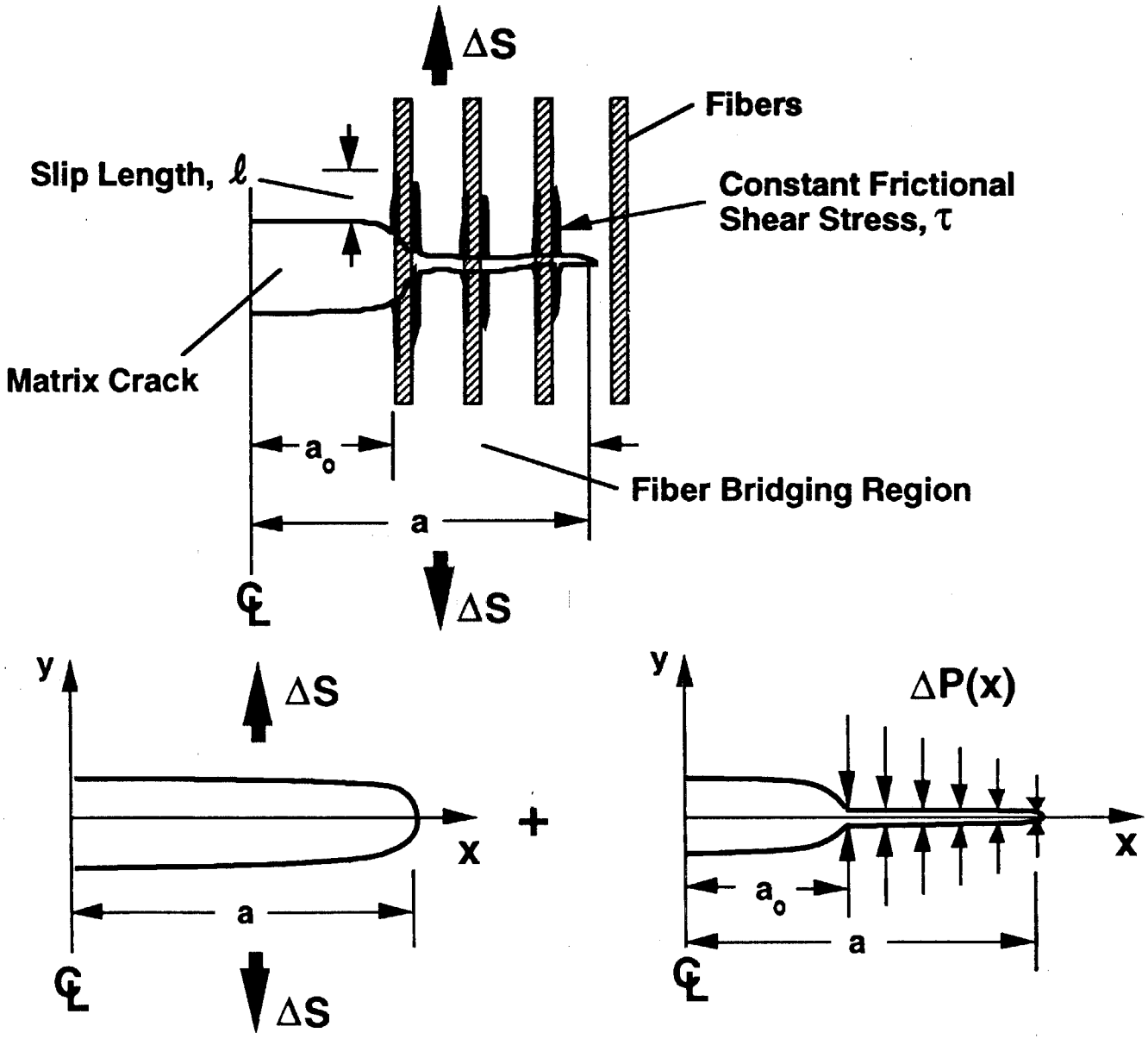

Figure 1. Continuum fracture mechanics approximation of matrix crack growth process during fatigue loading in TMC. Fibers bridging crack are idealized as a closure pressure. Governing equation is formulated by superposition of a crack subjected to a far-field applied stress and a crack subjected to a closure pressure.

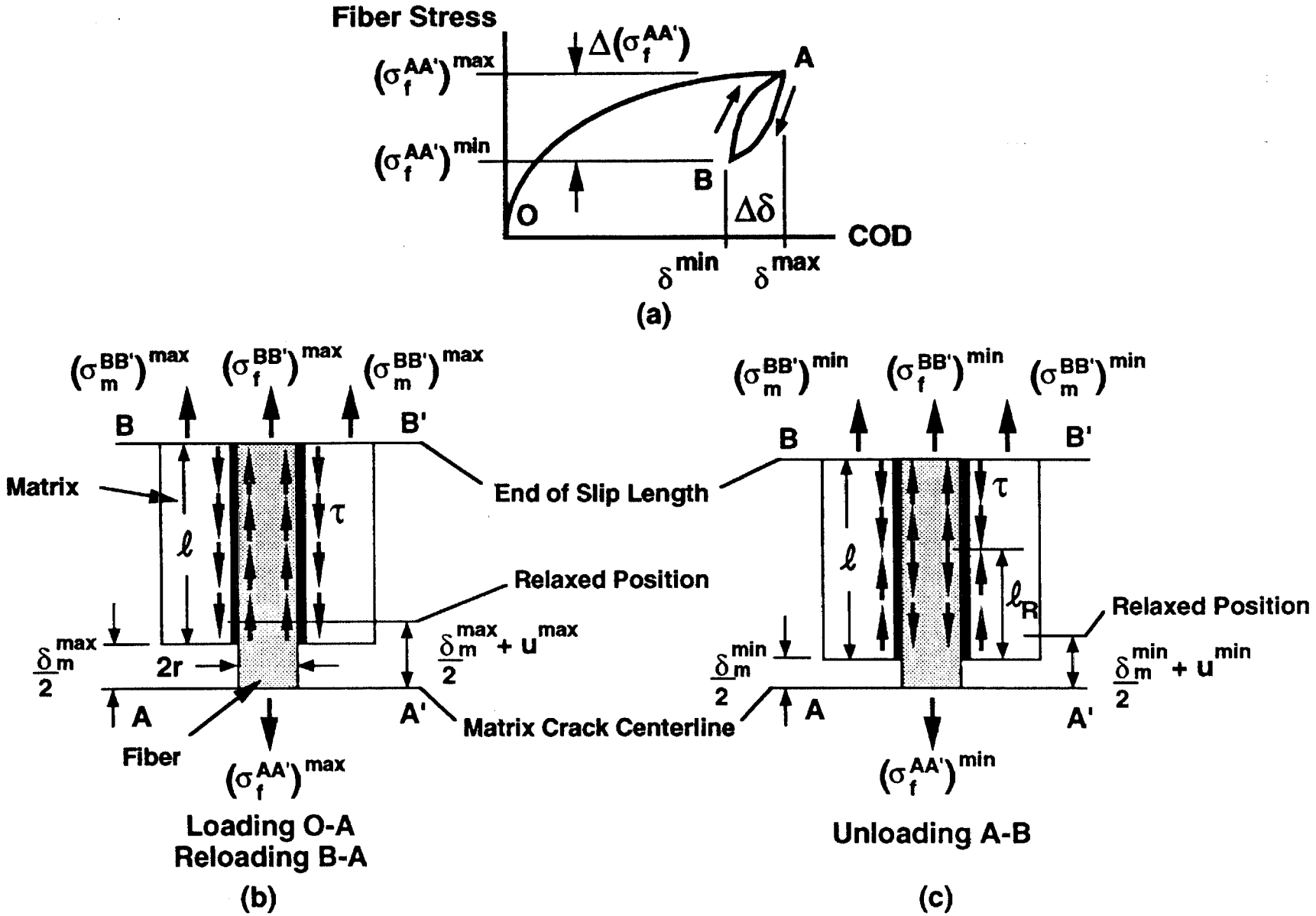

Figure 2. Micromechanics of fiber bridging: (a) Fiber stress as a function of crack opening displacement; (b) Free body diagram of fiber in wake of crack at maximum applied load; and (c) Free body diagram of fiber in wake of crack at minimum applied load.

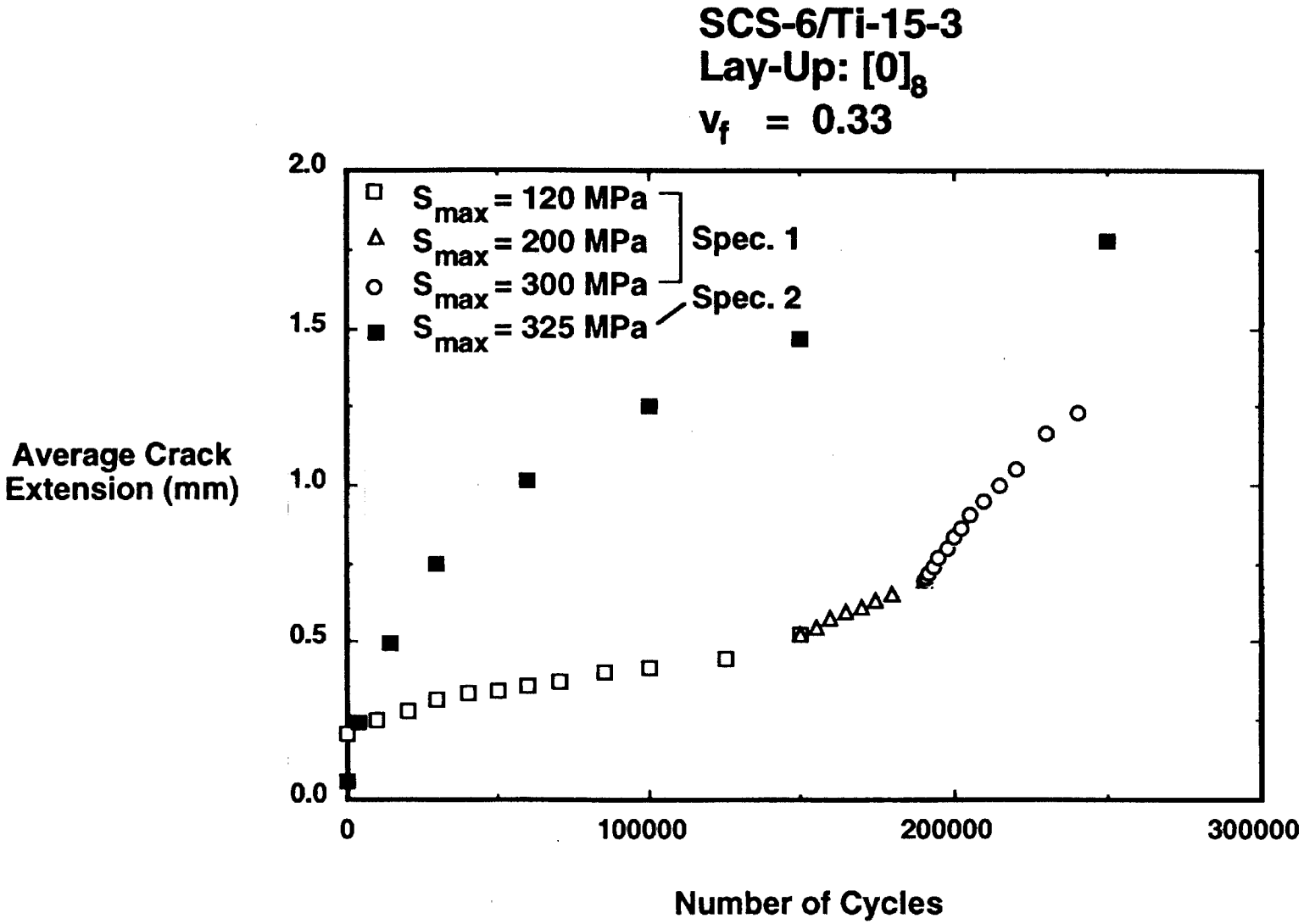

Figure 3. Average cumulative crack extension as a function of the number of fatigue cycles. As the number of cycles increases, the rate of crack growth decreases due to fibers bridging the matrix crack.

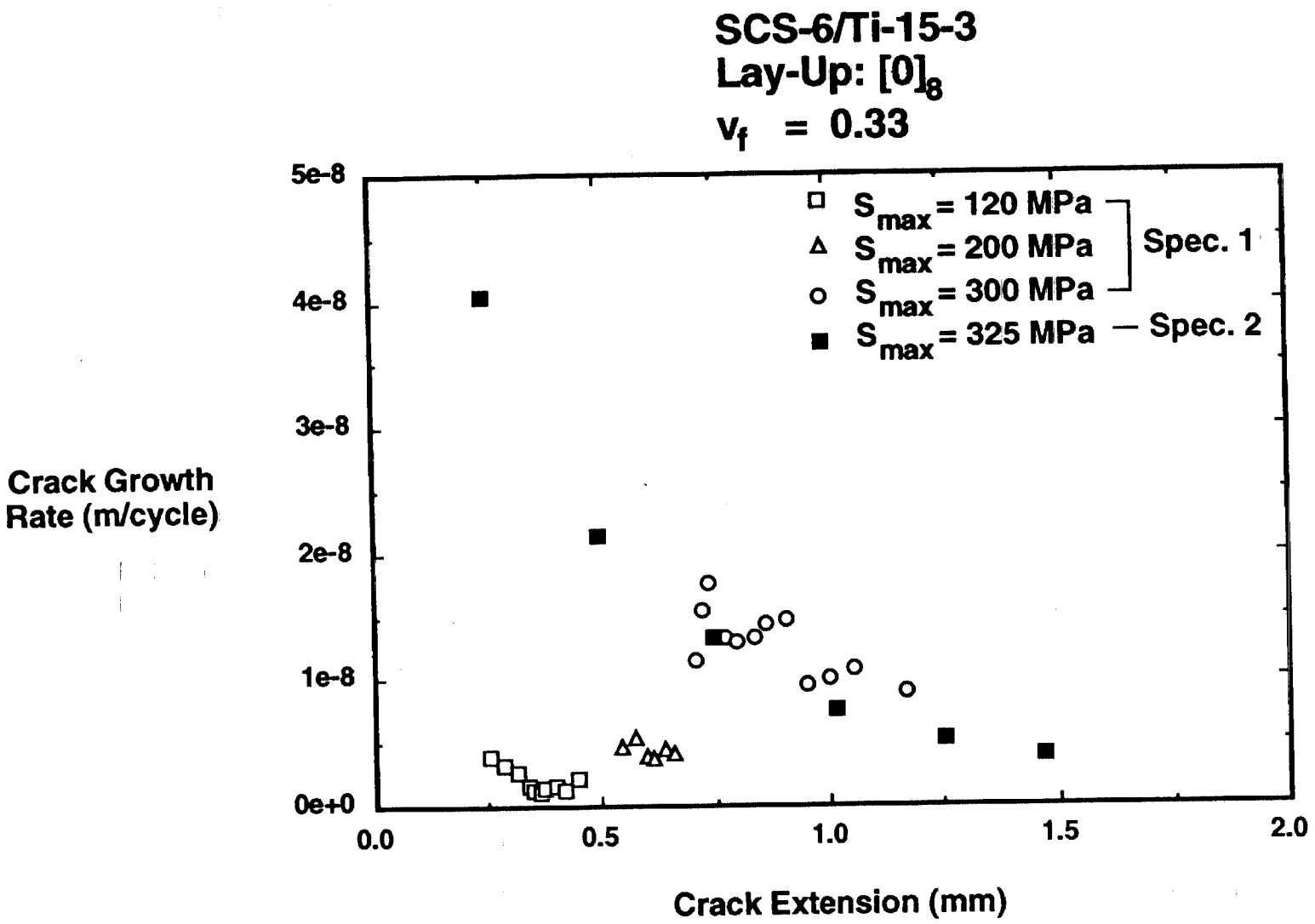

Figure 4. Crack growth rate as a function of the crack extension. As the matrix crack length increases, the rate of crack growth decreases due to fibers bridging the matrix crack.

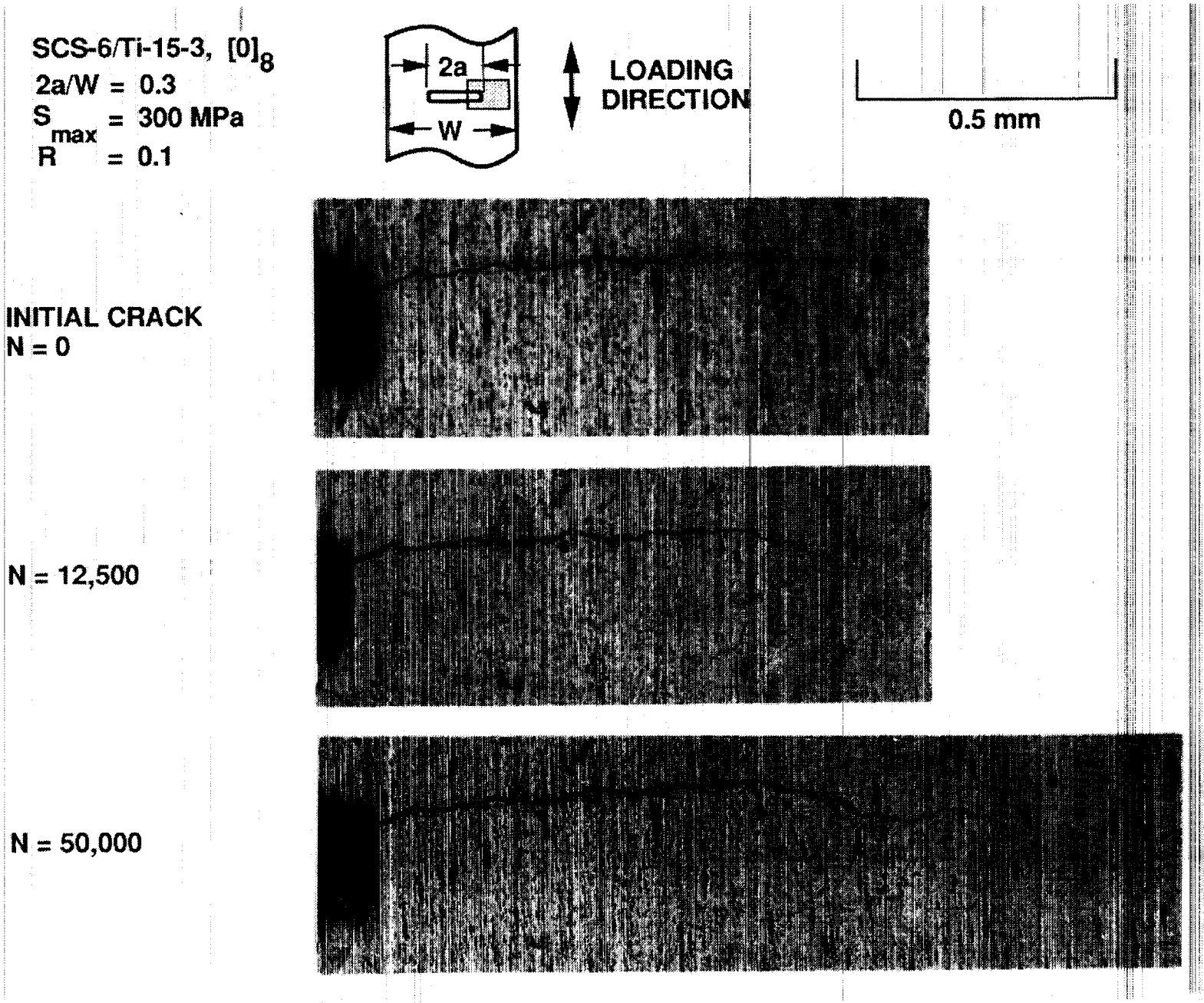

Figure 5. Development of notch-tip matrix cracks during fatigue loading, $v_f = 0.33$.

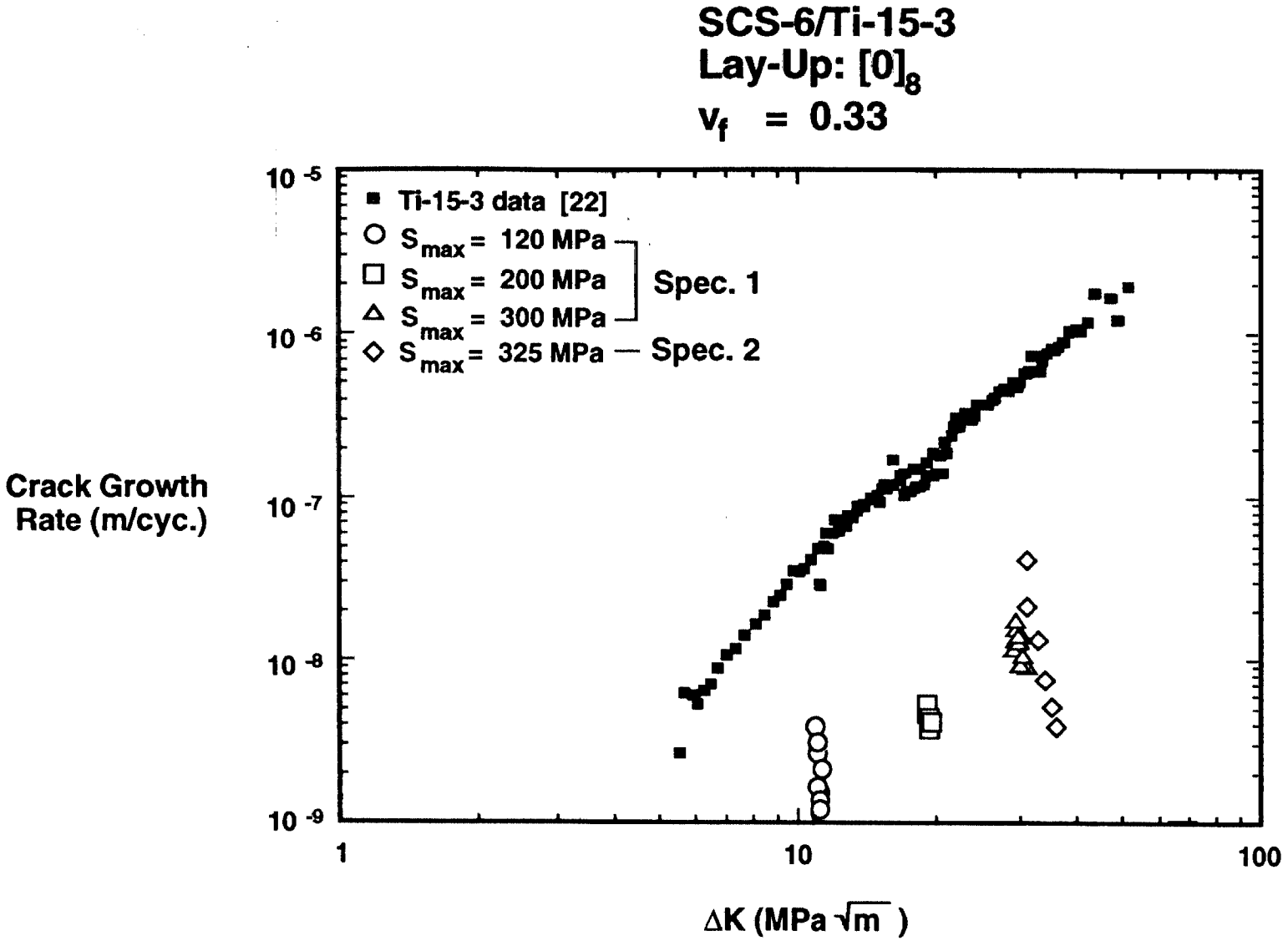

Figure 6. Crack growth rate as a function of the applied stress intensity factor range. The applied stress intensity factor range overestimates the stress intensity factor range in the matrix and, therefore, cannot be used to characterize matrix crack growth.

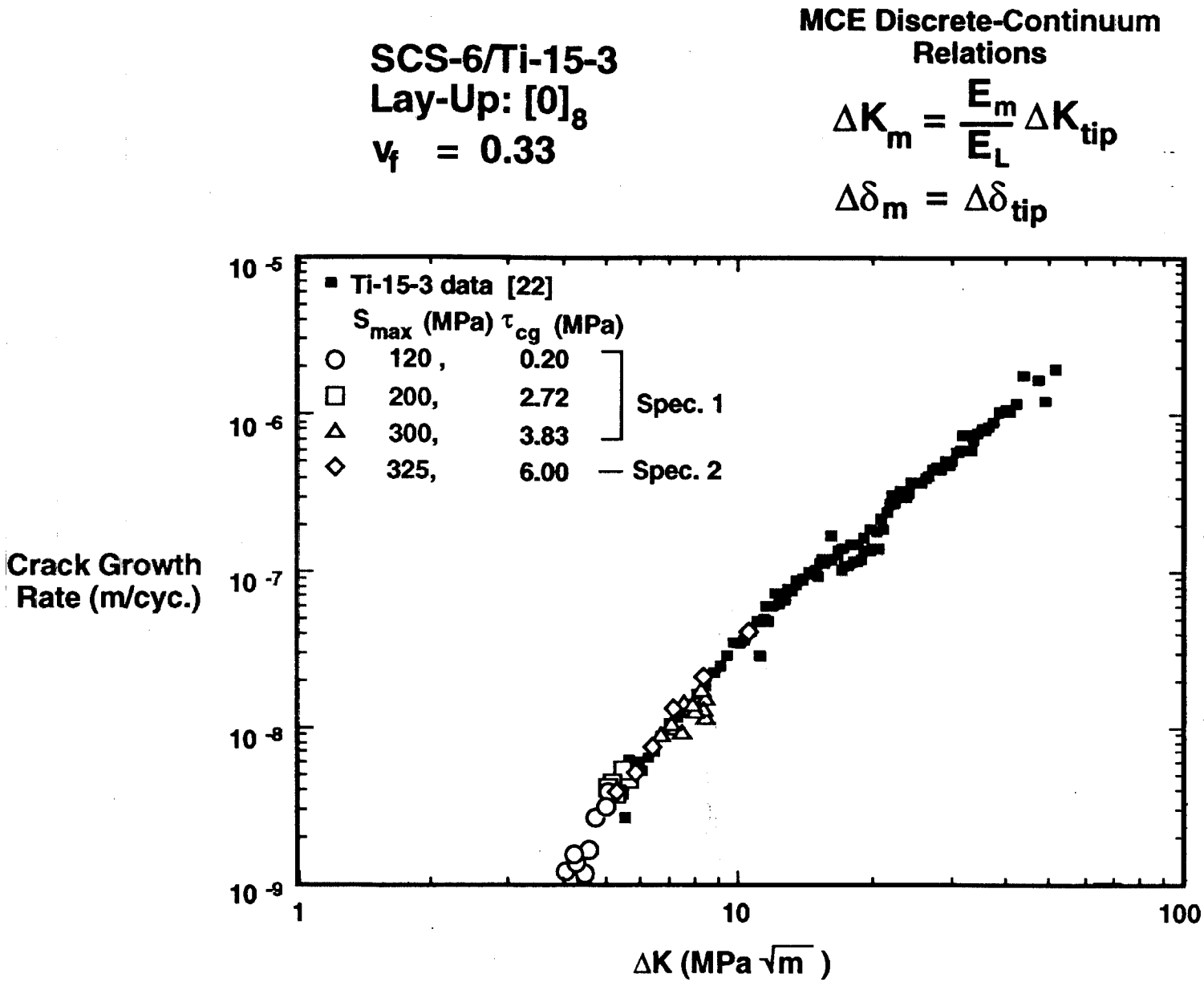

Figure 7. Crack growth rate as a function of stress intensity factor range for given values of applied stress. The stress intensity factor range in the matrix was calculated using the MCE discrete-continuum relations for the given values of τ_{cg}.

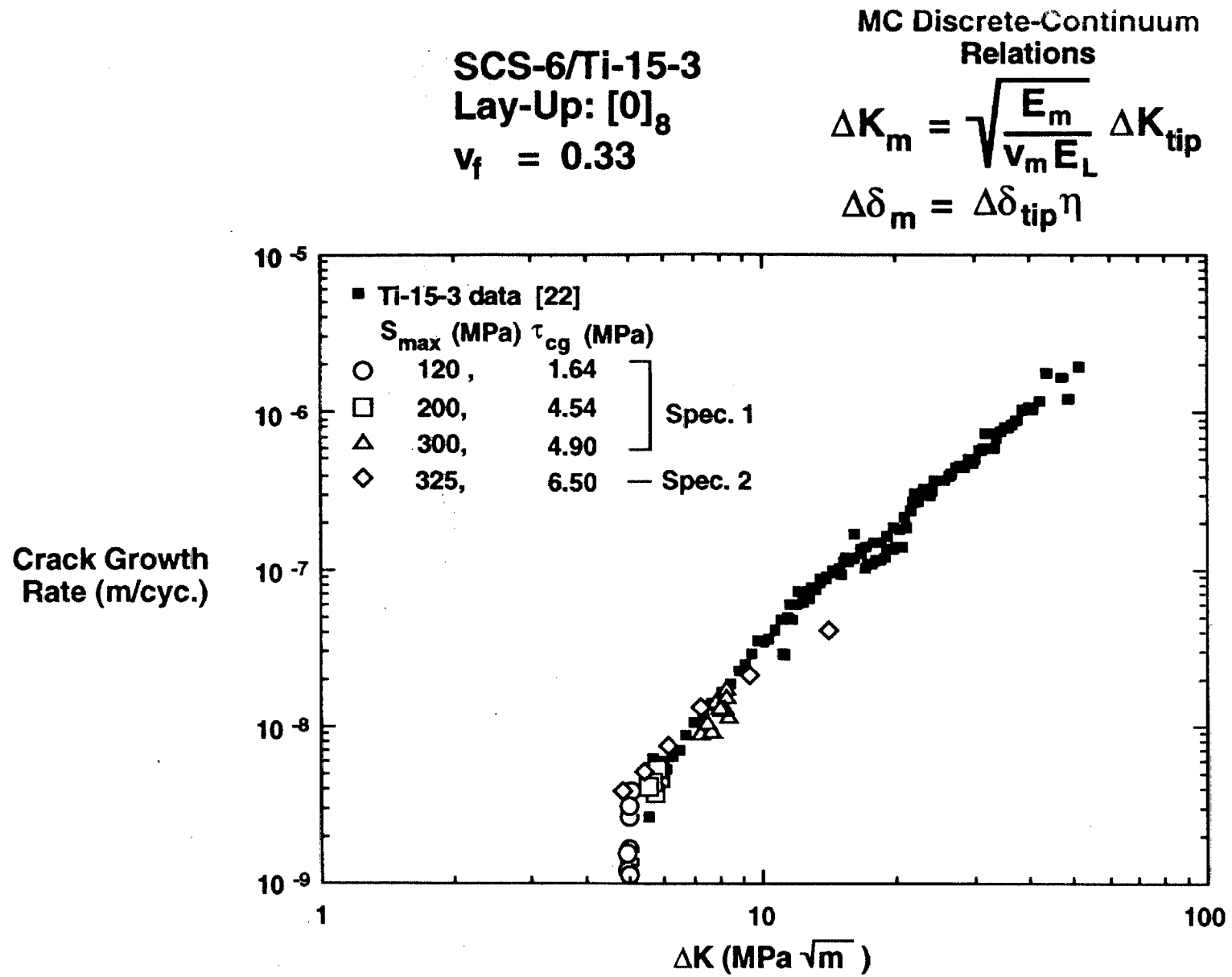

Figure 8. Crack growth rate as a function of stress intensity factor range for given values of applied stress. The stress intensity factor range in the matrix was calculated using the MC discrete-continuum relations for the given values of τ_{cg}.

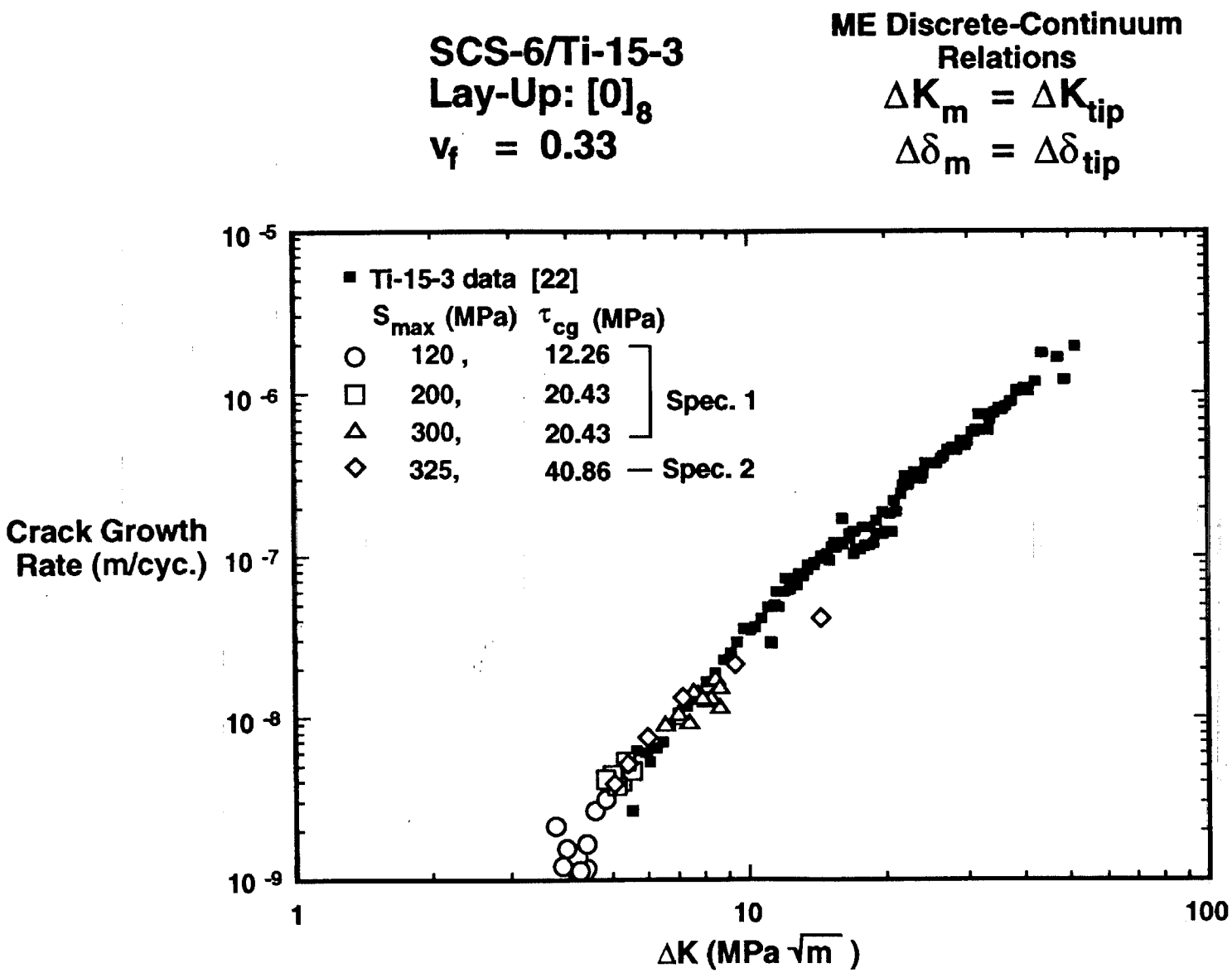

Figure 9. Crack growth rate as a function of stress intensity factor range for given values of applied stress. The stress intensity factor range in the matrix was calculated using the ME discrete-continuum relations for the given values of τ_{cg}.

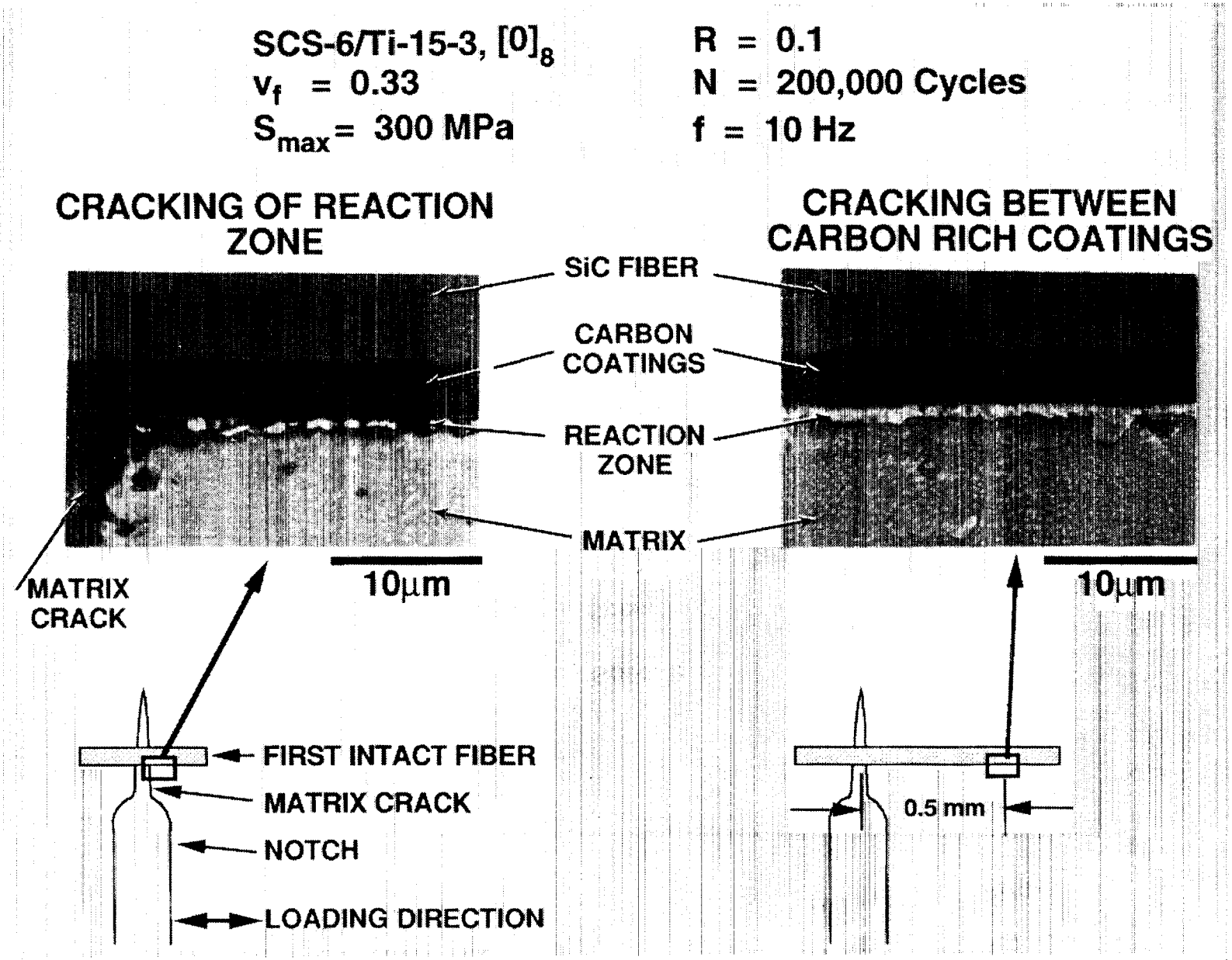

Figure 10. Mechanisms of fiber-matrix debonding along the first intact fiber. Close to the matrix crack, debonding consisted of fracture of the brittle reaction zone. At approximately 0.5 mm from the matrix crack, debonding consisted of cracking between the carbon rich coatings.

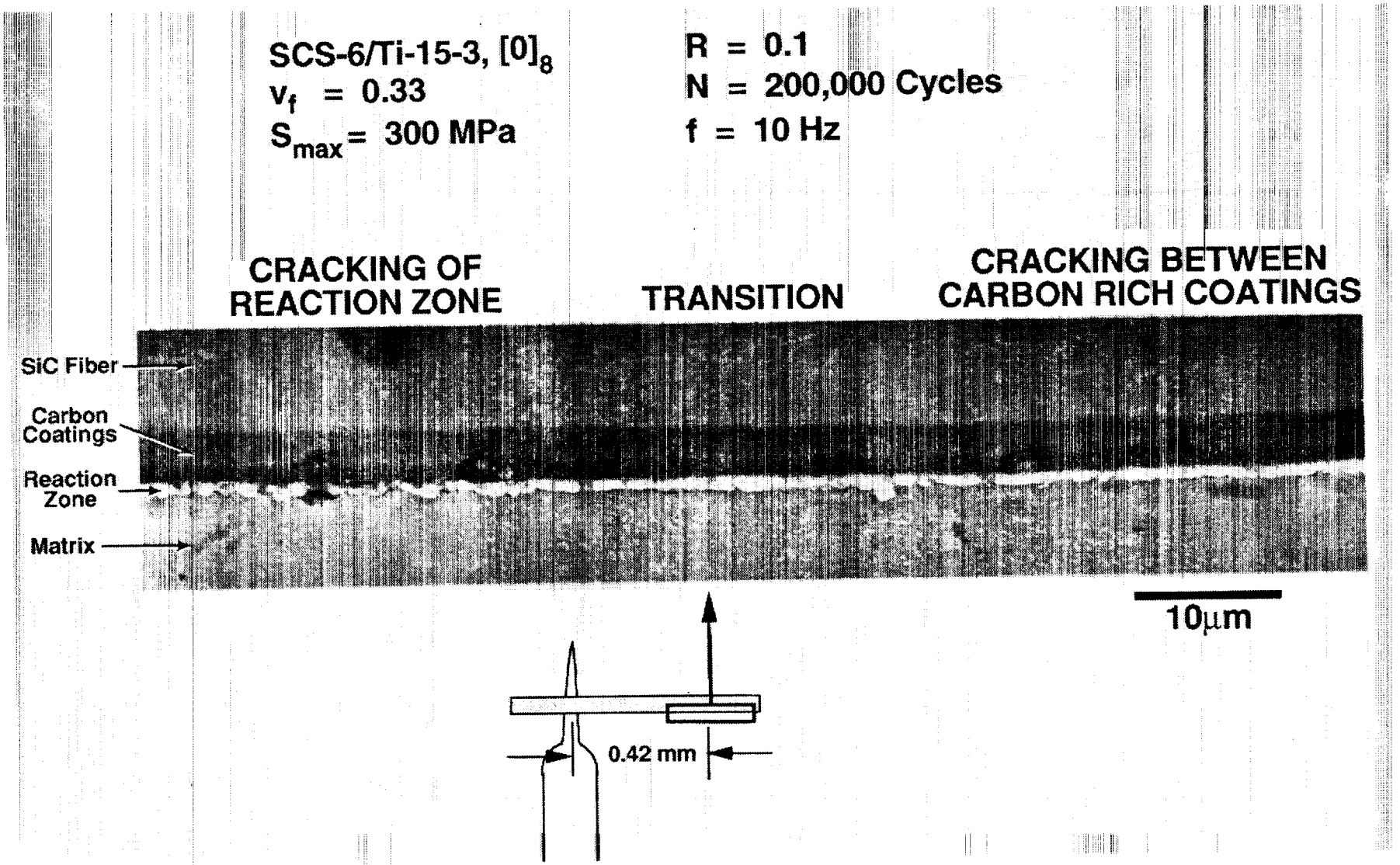

Figure 11. Mechanisms of fiber-matrix debonding along the first intact fiber. Transistion of fiber-matrix debonding mechanisms occurred at approximately 0.42 mm from the matrix crack.

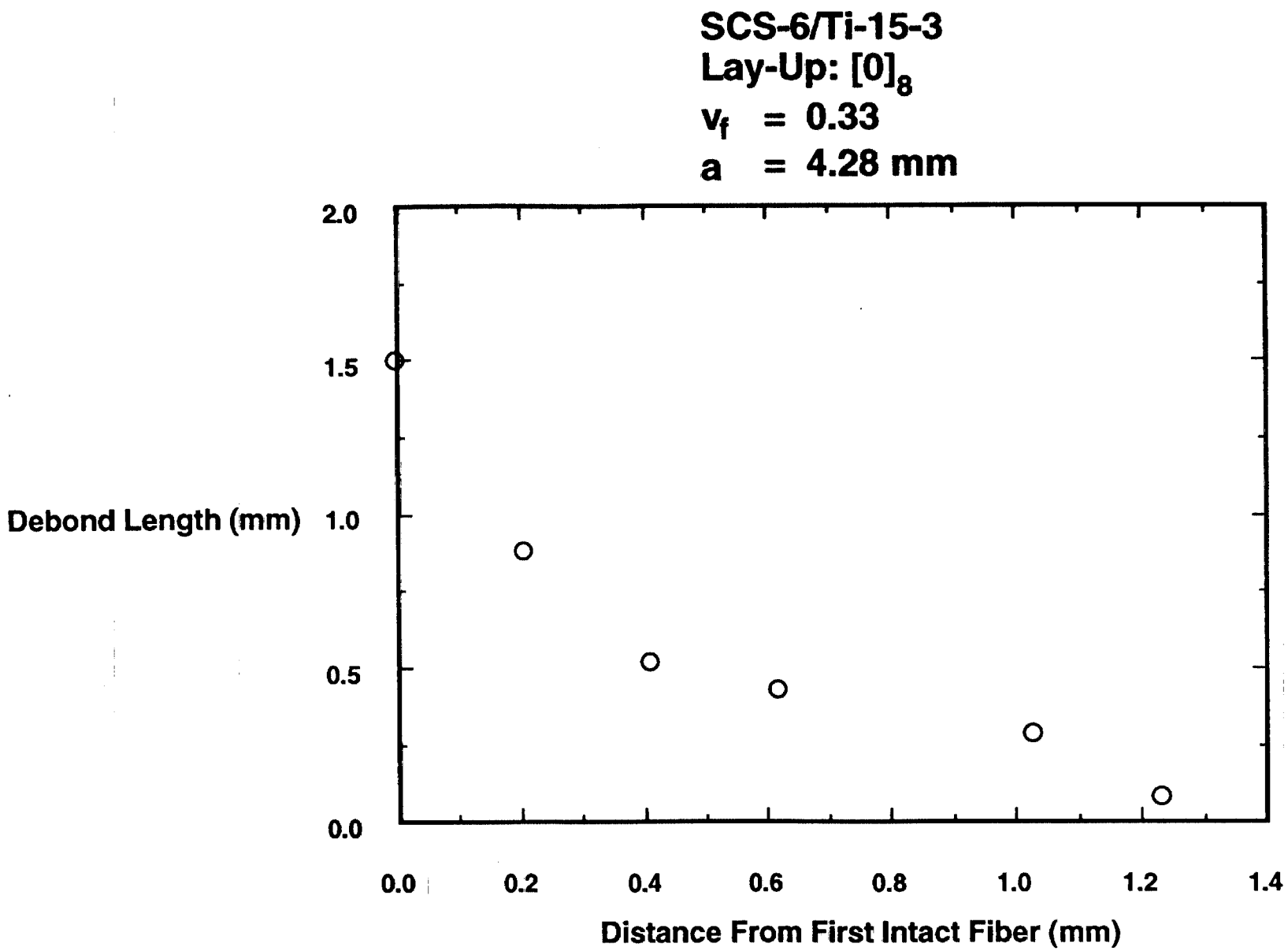

Figure 12. Debond length measured in each fiber in the bridging region. The debond length decreases as the distance from the first intact fiber increases.

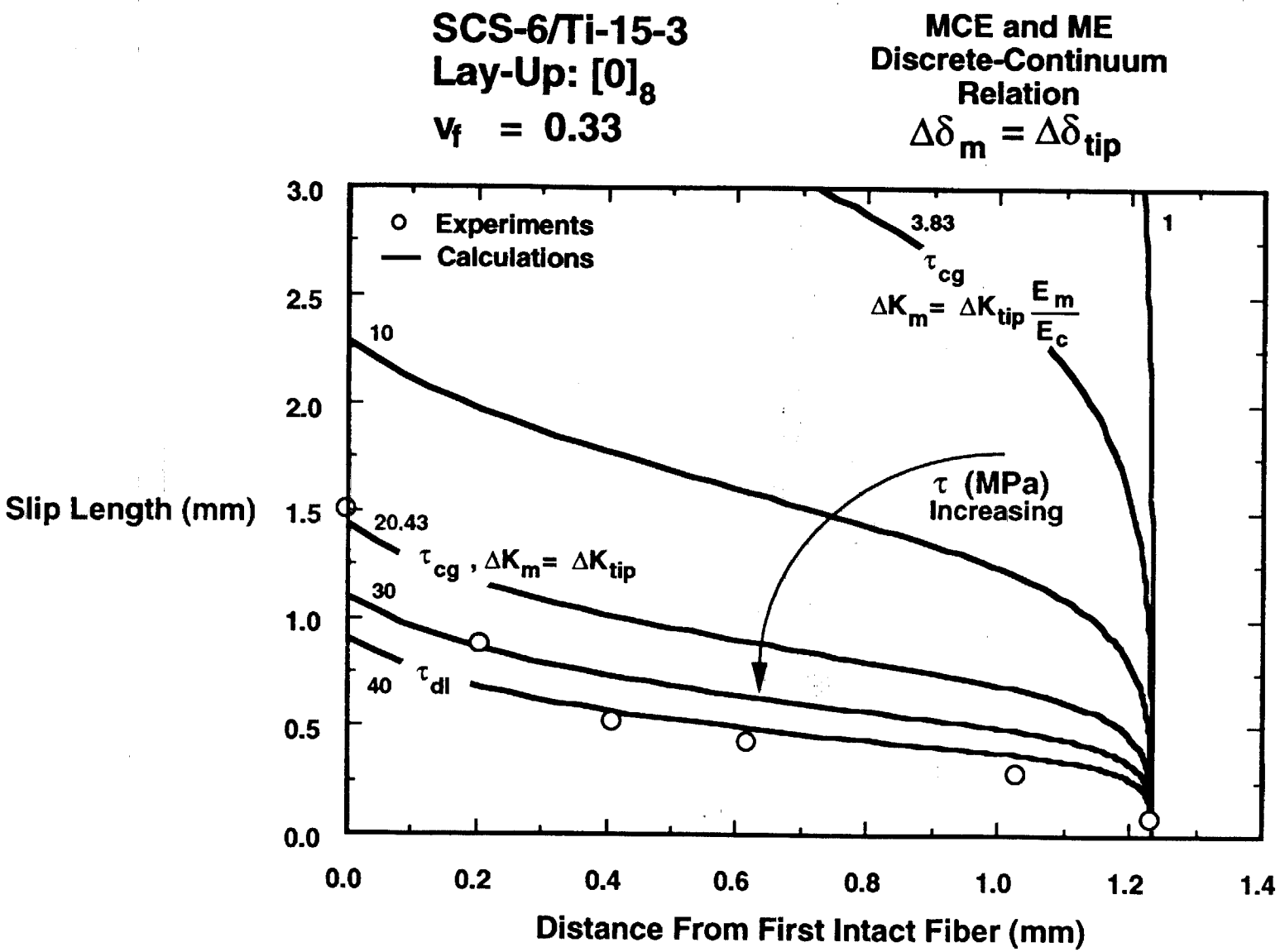

Figure 13. Slip length calculated using the MCE and ME displacement relations for given values of τ. As τ increases, the slip length decreases. Best agreement between experiments and calculations was obtained for τ_{dl} = 40 MPa.

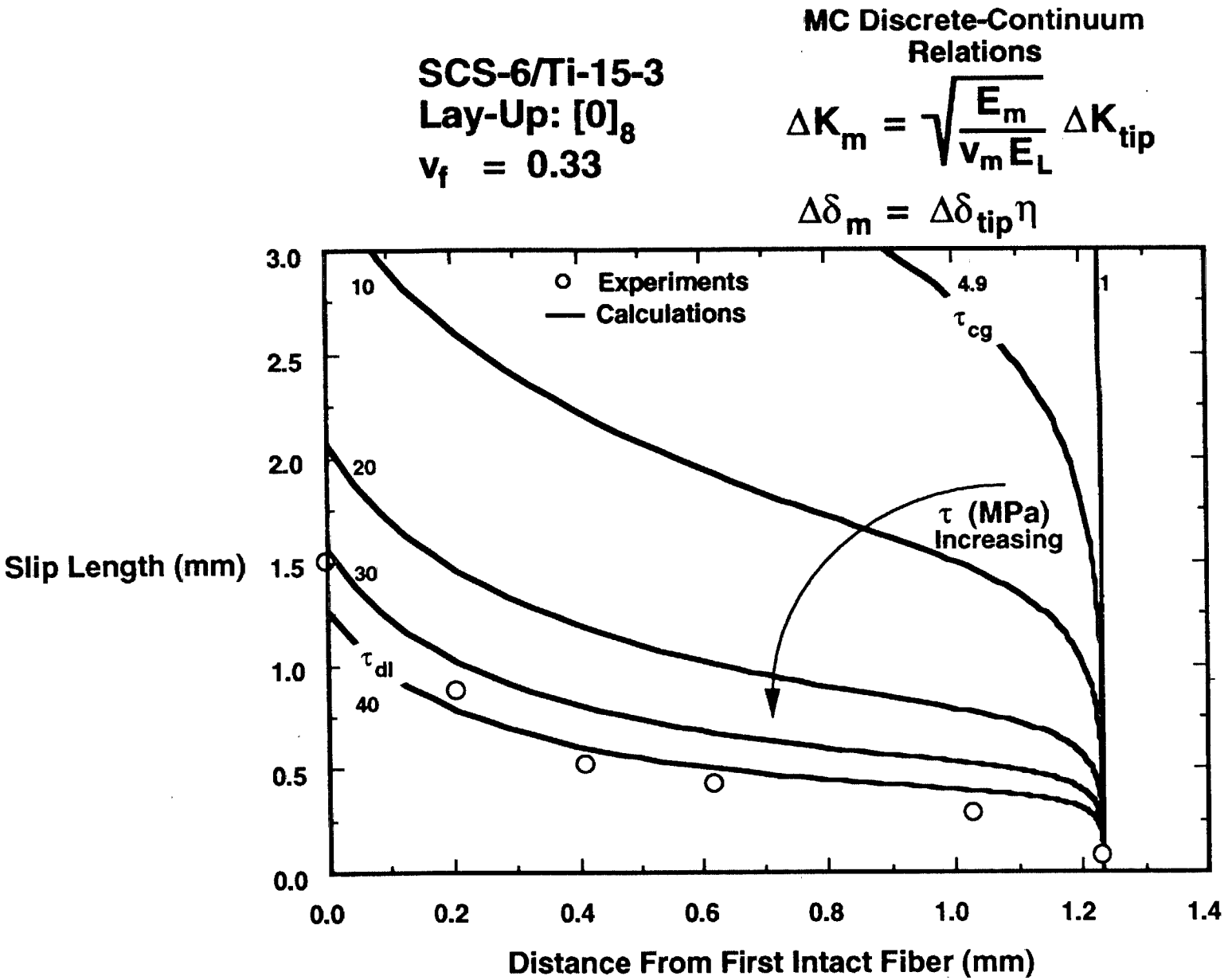

Figure 14. Slip length calculated using the MC discrete-continuum relations for given values of τ. As τ increases, the slip length decreases. Best agreement between experiments and calculations was obtained for τ_{dl} = 40 MPa.

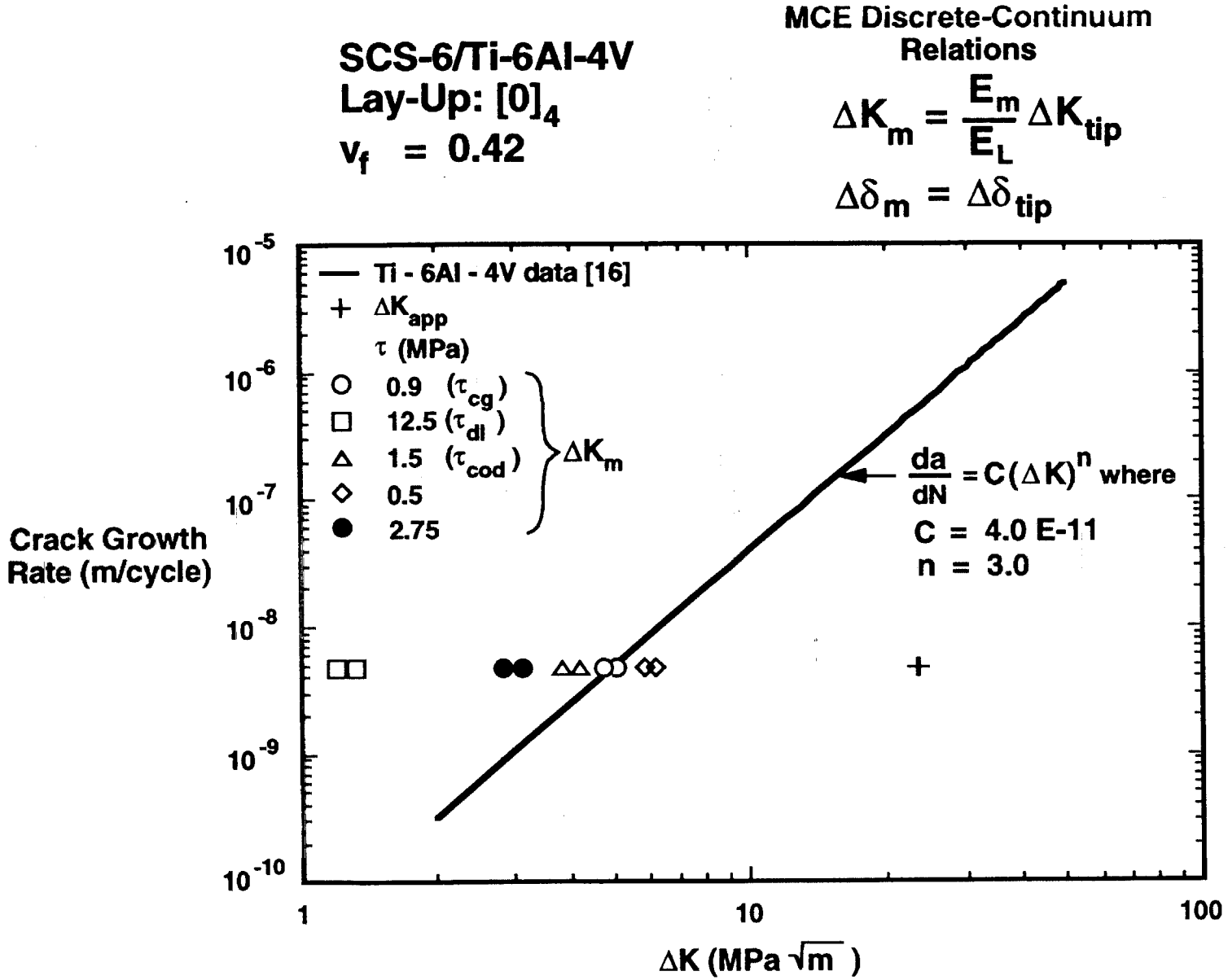

Figure 15. Crack growth rate as a function of stress intensity factor range. The applied stress intensity factor range overestimates the ΔK governing matrix crack growth. Using the MCE discrete-continuum relations, ΔK_m was calculated for given values of τ. Best agreement between experiments and calculations was obtained for τ_{cg}= 0.9 MPa.

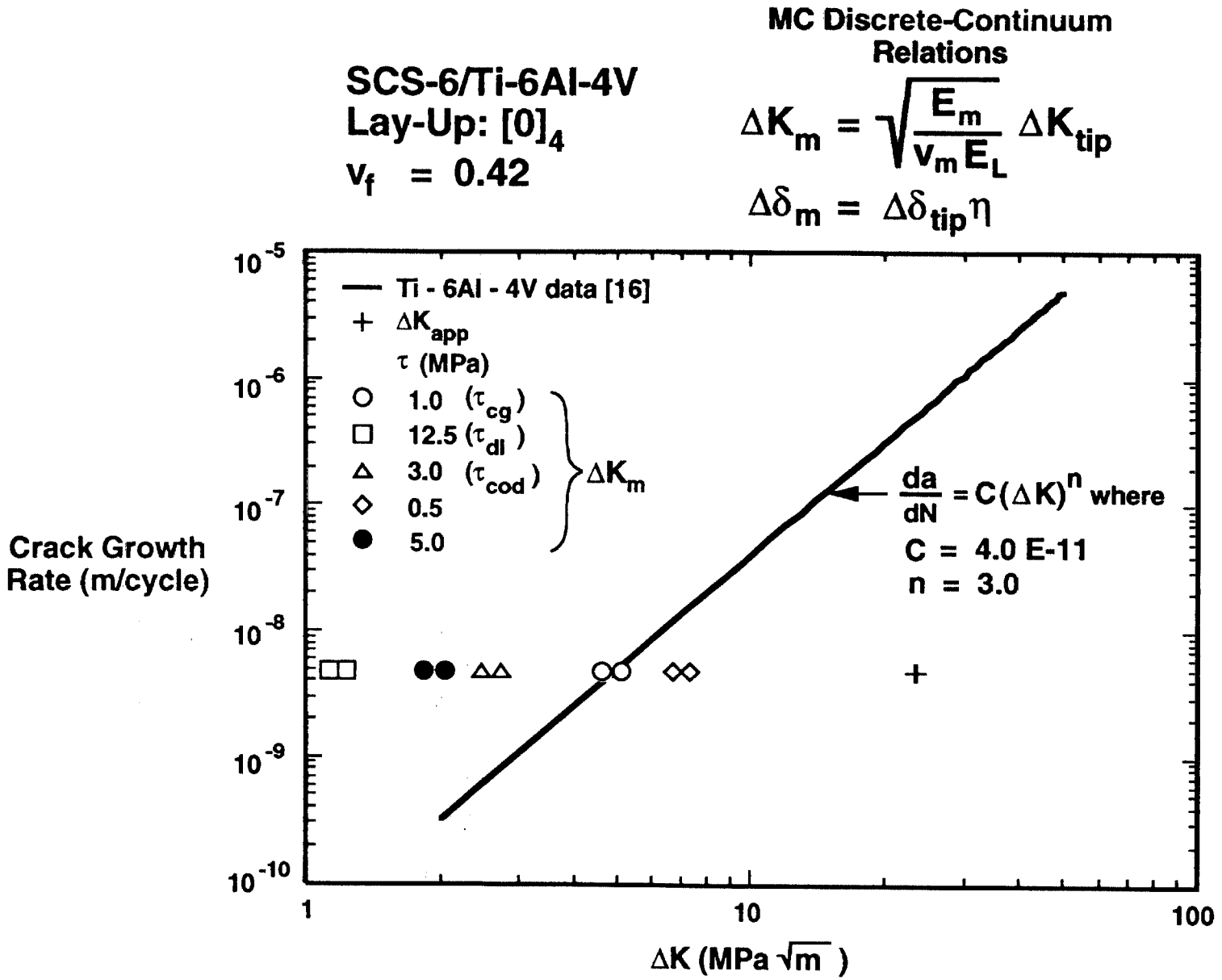

Figure 16. Crack growth rate as a function of stress intensity factor range. The applied stress intensity factor range overestimates the ΔK governing matrix crack growth. Using the MC discrete-continuum relations, ΔK_m was calculated for given values of τ. Best agreement between experiments and calculations was obtained for τ_{cg}= 1.0 MPa.

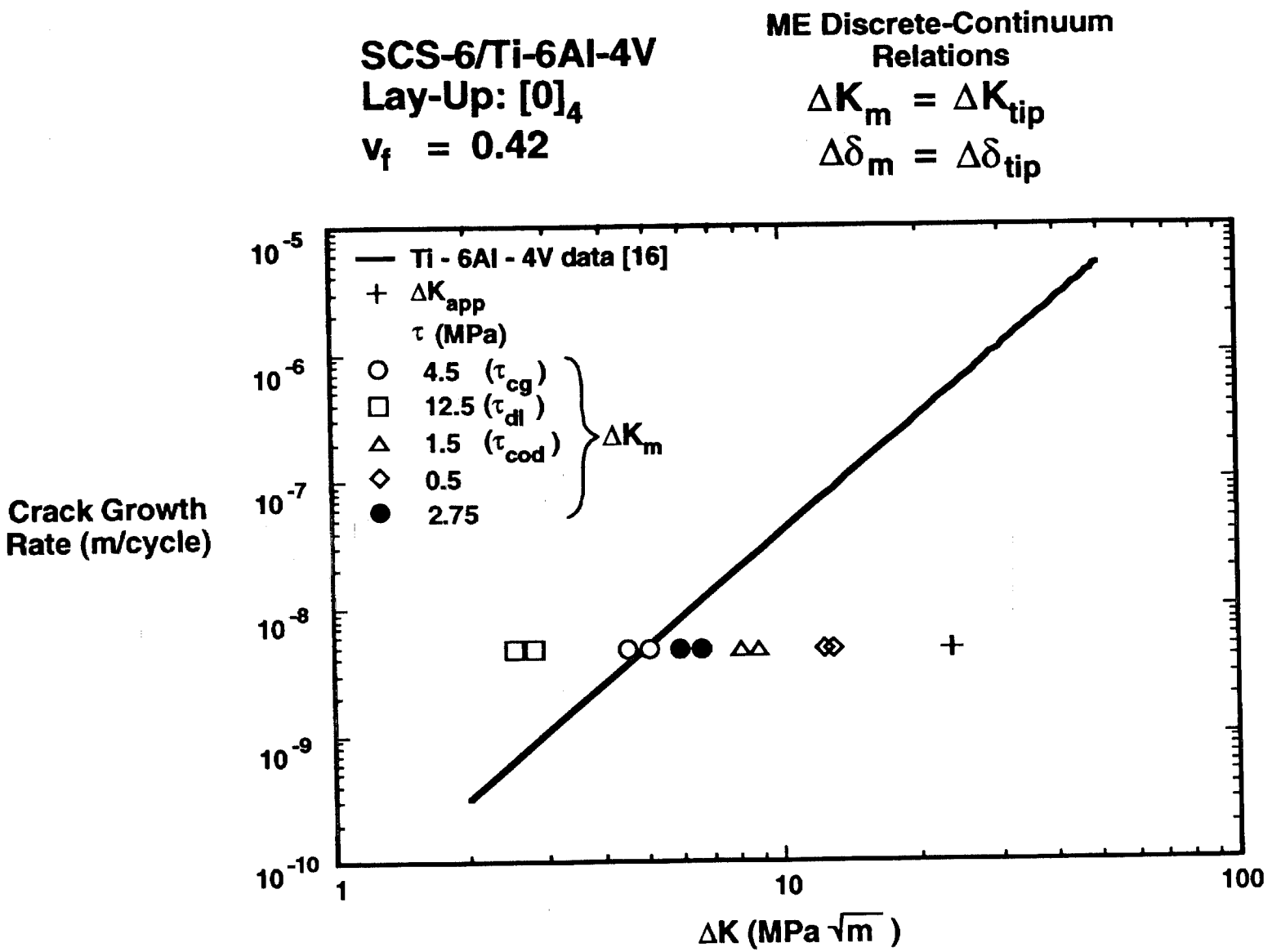

Figure 17. Crack growth rate as a function of stress intensity factor range. The applied stress intensity factor range overestimates the ΔK governing matrix crack growth. Using the ME discrete-continuum relations, ΔK_m was calculated for given values of τ. Best agreement between experiments and calculations was obtained for τ_{cg}= 4.5 MPa.

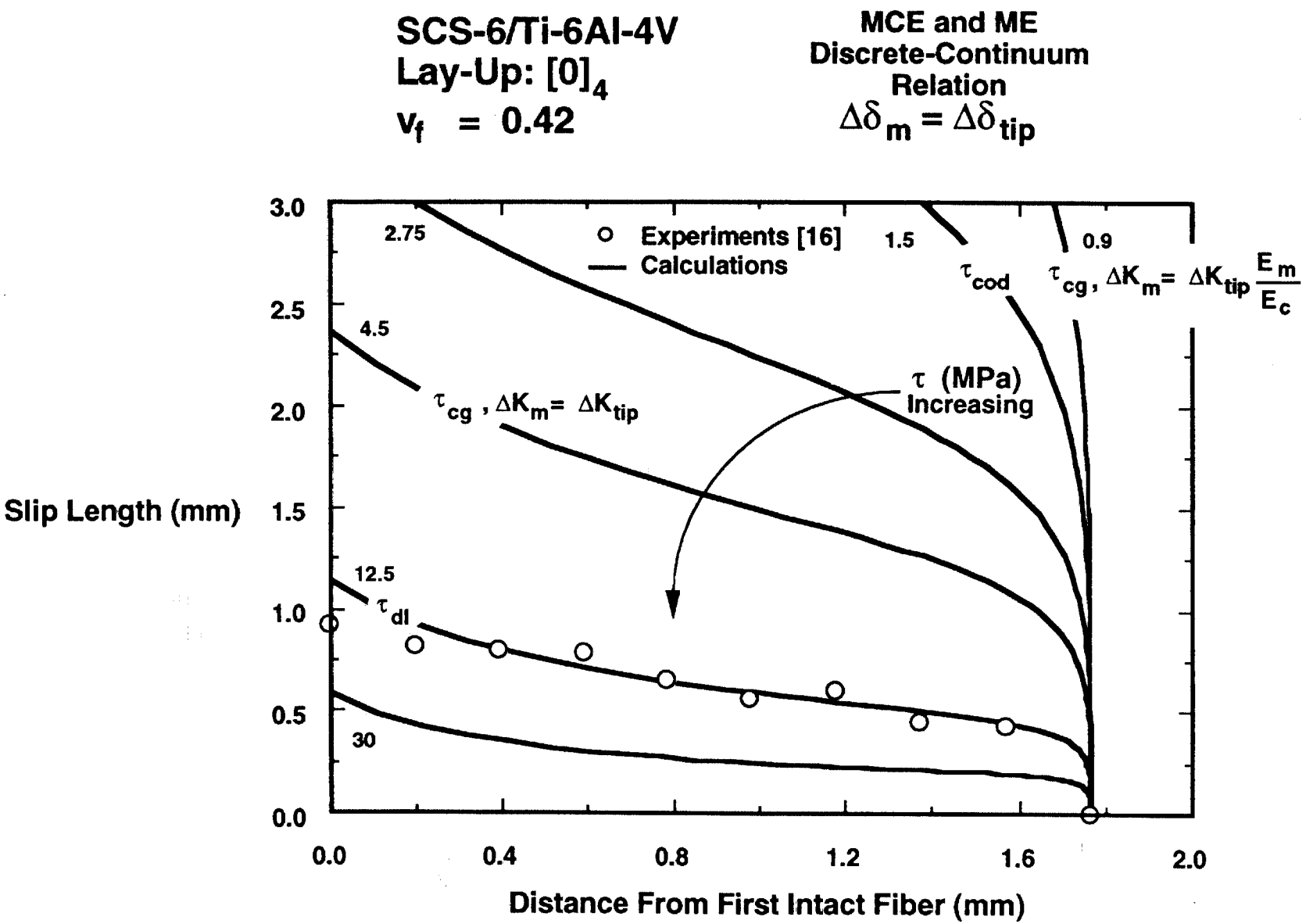

Figure 18. Slip length calculated using the MCE and ME displacement relations for given values of τ. As τ increases, the slip length decreases. Best agreement between experiments and calculations was obtained for τ_{dl} = 12.5 MPa.

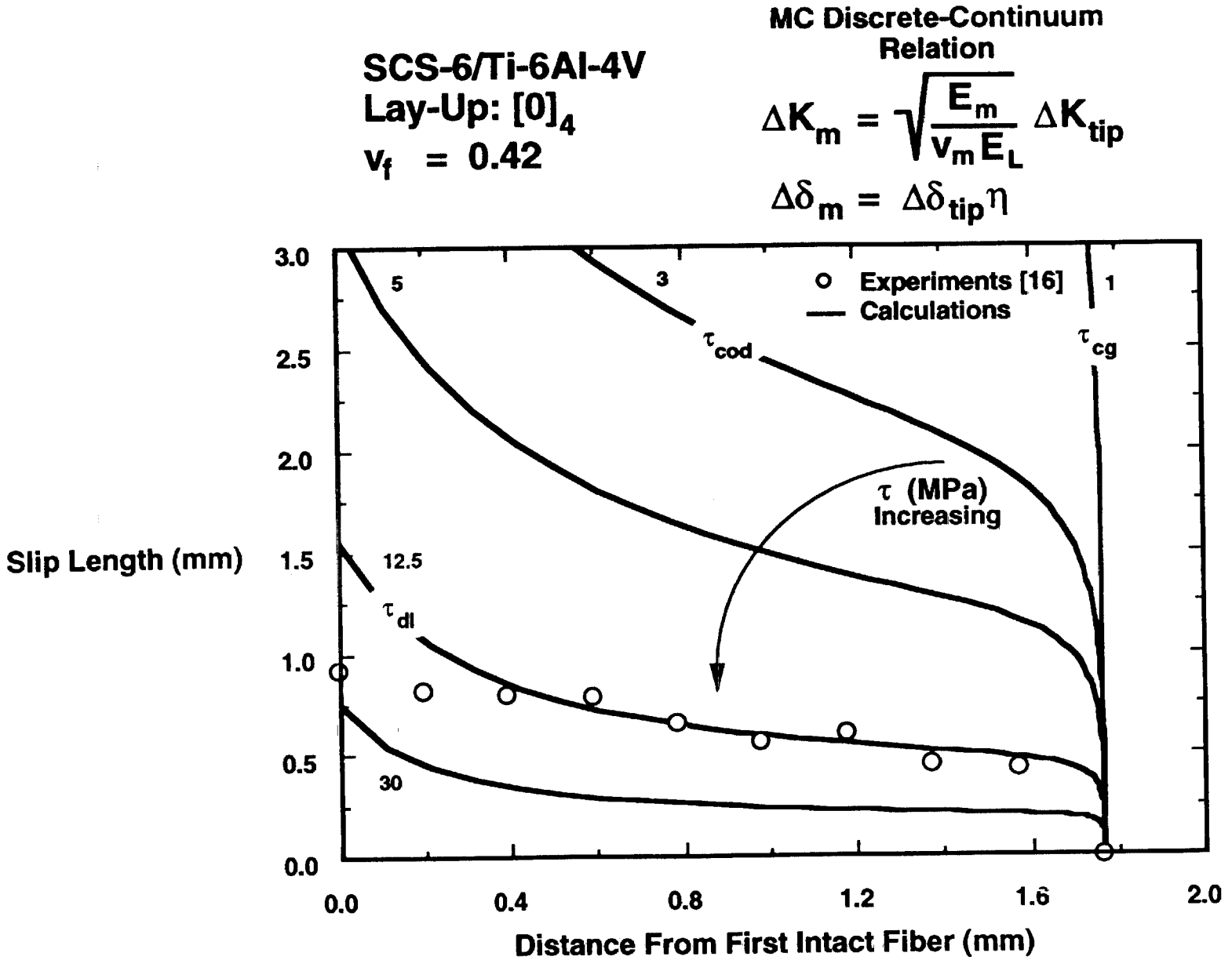

Figure 19. Slip length calculated using the MC discrete-continuum relations for given values of τ. As τ increases, the slip length decreases. Best agreement between experiments and calculations was obtained for τ_{dl} = 12.5 MPa.

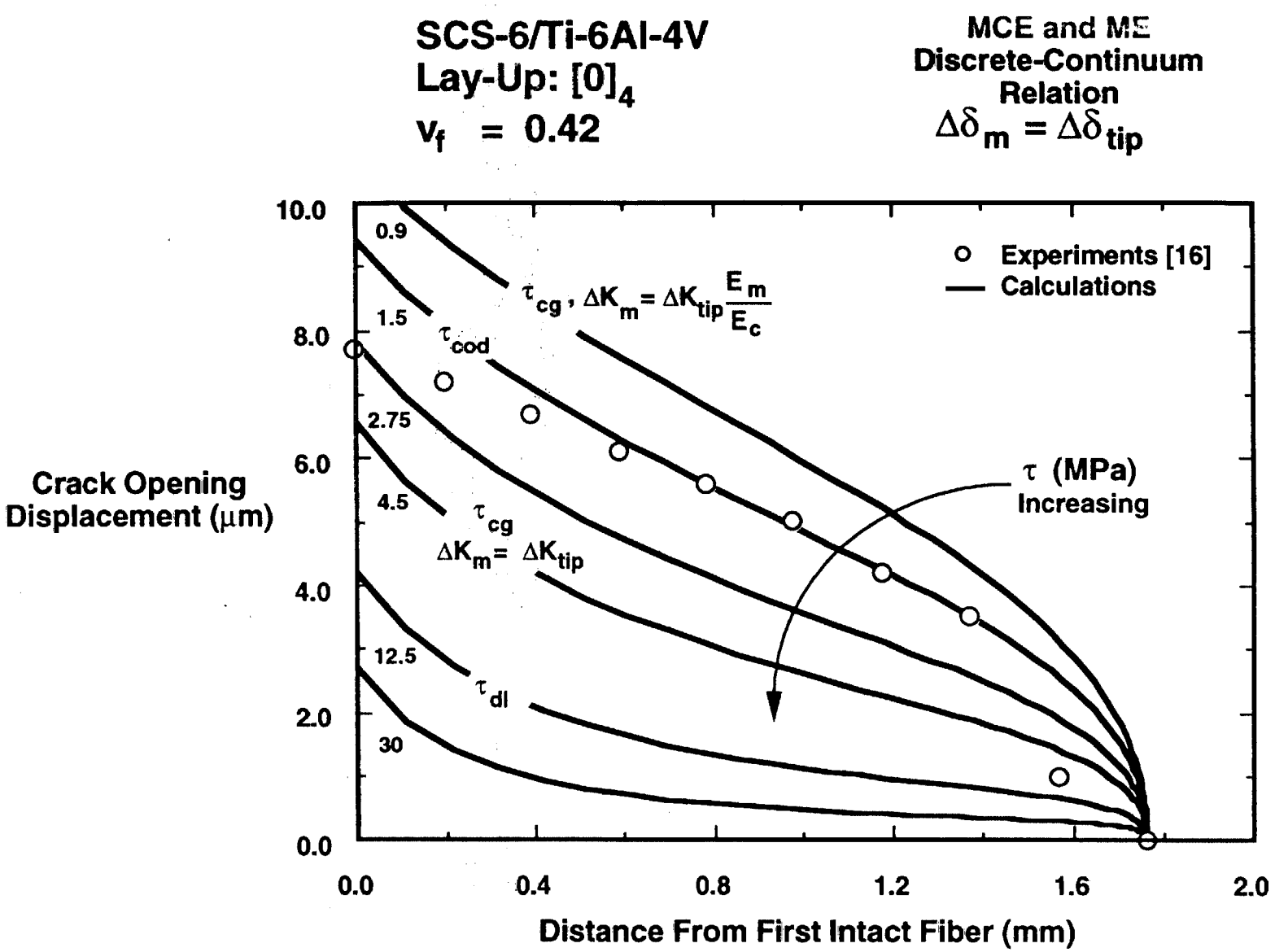

Figure 20. Crack opening displacement calculated using the MCE and ME displacement relation for given values of τ. As τ increases, the crack opening displacement decreases. Best agreement between experiments and calculations was obtained for τ_{cod}= 1.5 MPa.

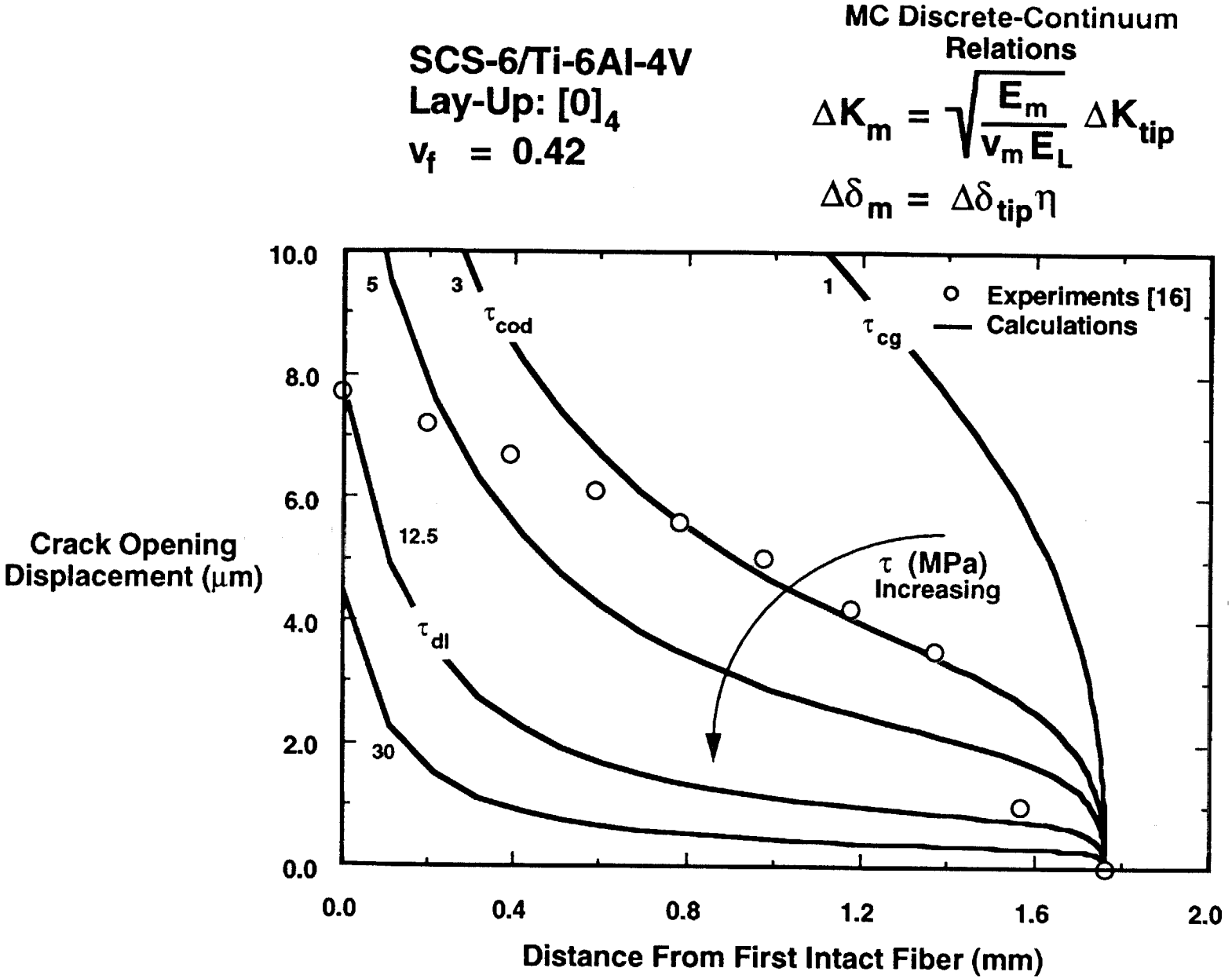

Figure 21. Crack opening displacement calculated using the MC discrete-continuum relations for given values of τ. As τ increases, the crack opening displacement decreases. Best agreement between experiments and calculations was obtained for τ_{cod}= 3.0 MPa.

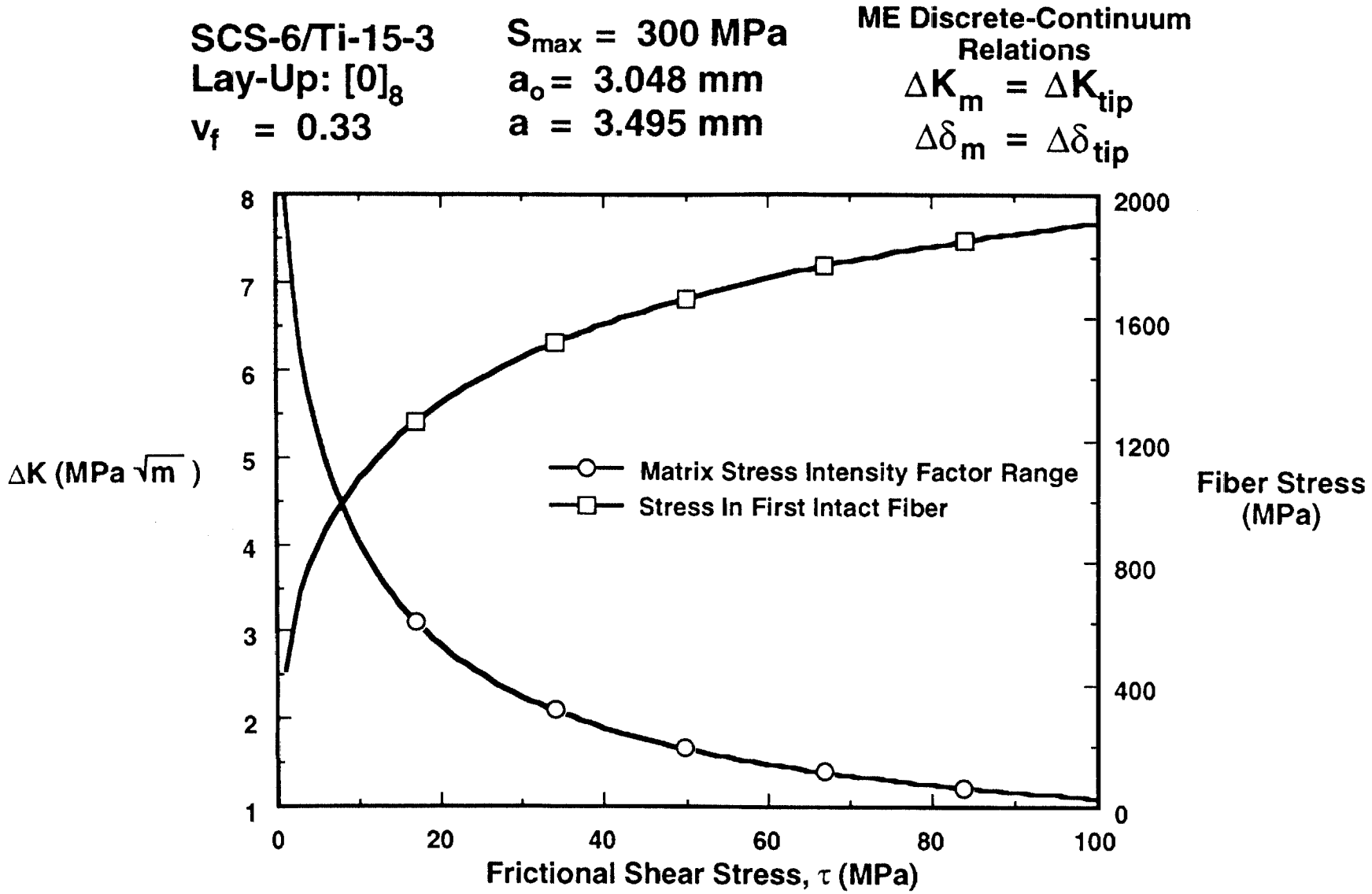

Figure 22. Stress intensity factor range in matrix and stress in first intact fiber as a function of the interfacial frictional shear. As τ increases, the stress in the first intact fiber increases, thus, promoting fiber breakage. As τ decreases, the matrix stress intensity factor range increases, thus, promoting matrix cracking.

REPORT DOCUMENTATION PAGE

Form Approved
OMB No 0704-0188

1. AGENCY USE ONLY (Leave blank)	2. REPORT DATE	3. REPORT TYPE AND DATES COVERED
	July 1992	Technical Memorandum

4. TITLE AND SUBTITLE
Application of Fiber Bridging Models to Fatigue Crack Growth in Unidirectional Titanium Matrix Composites

5. FUNDING NUMBERS
WU 763-23-41-85

6. AUTHOR(S)
J. G. Bakuckas, Jr. and W. S. Johnson

7. PERFORMING ORGANIZATION NAME(S) AND ADDRESS(ES)
NASA Langley Research Center
Hampton, VA 23665-5225

8. PERFORMING ORGANIZATION REPORT NUMBER

9. SPONSORING / MONITORING AGENCY NAME(S) AND ADDRESS(ES)
National Aeronautics and Space Administration
Washington, DC 20546

10. SPONSORING / MONITORING AGENCY REPORT NUMBER
NASA TM-107588

11. SUPPLEMENTARY NOTES
Bakuckas: Resident Research Associate, National Research Council, NASA Langley Research Center, Hampton, VA;
Johnson: Senior Research Engineer, NASA Langley Research Center, Hampton, VA

12a. DISTRIBUTION / AVAILABILITY STATEMENT
Unclassified - Unlimited

Subject Category - 39

12b. DISTRIBUTION CODE

13. ABSTRACT *(Maximum 200 words)*
Several fiber bridging models were reviewed and applied in this research to study the matrix fatigue crack growth behavior in center notched [0]8 SCS-6/Ti-15-3 and [0]4 SCS-6/Ti-6Al-4V laminates. Observaions revealed that fatigue damage consisted primarily of matrix cracks and fiber-matrix interfacial failure in the [0]8 SCS-6/Ti-15-3 laminates. Fiber-matrix interface failure included fracture of the brittle reaction zone and cracking between the two carbon rich fiber coatings. Intact fibers in the wake of the matrix cracks reduce the stress intensity factor range. Thus, an applied stress intensity factor range ($\Delta K_{app} = \Delta S\sqrt{\pi a}$) is inappropriate to characterize matrix crack growth behavior. Fiber bridging models were used to determine the matrix stress intensity factor range in titanium metal matrix composites. In these models, the fibers in the wake of the crack are idealized as a closure pressure. An unknown constant frictional shear stress is assumed to act along the debond or slip length of the bridging fibers. In this study, the frictional shear stress was used as a curve fitting parameter to available data (crack growth data, crack opening displacement data, and debond length data) Large variations in the frictional shear stress required to fit the experimental data indicate that the fiber bridging models in their present form lack predictive capabilities. However, these models provide an efficient and relatively simple engineering method for conducting parametric studies of the matrix crack growth behavior based on constituent properties.

14. SUBJECT TERMS	15. NUMBER OF PAGES
Matrix cracking; Fiber-matrix debonding; Matrix stress intensity factor Continuum fracture mechanics; Micromechanics	53
	16. PRICE CODE A05

17. SECURITY CLASSIFICATION OF REPORT	18. SECURITY CLASSIFICATION OF THIS PAGE	19. SECURITY CLASSIFICATION OF ABSTRACT	20. LIMITATION OF ABSTRACT
Unclassified	Unclassified		